SOME ANELASTIC PROPERTIES OF ZIRCONIUM RESULTING FROM PRESTRAIN AT 77°K

By

EDWARD PHILIP DAHLBERG

A DISSERTATION PRESENTED TO THE GRADUATE COUNCIL OF
THE UNIVERSITY OF FLORIDA
IN PARTIAL FULFILLMENT OF THE REQUIREMENTS FOR THE
DEGREE OF DOCTOR OF PHILOSOPHY

UNIVERSITY OF FLORIDA

April, 1967

ACKNOWLEDGEMENTS

It is a pleasure to thank my supervisory committee chairman, Dr. Robert E. Reed-Hill, for his assistance in defining the nature and scope of this research project. His continuing interest, guidance, and encouragement were invaluable. I gratefully acknowledge Dr. F. N. Rhines, Dr. R. T. DeHoff, Dr. J. J. Hren, Dr. R. W. Cowen, and Dr. J. Jahanshie for serving on my supervisory committee. Special thanks are due to Mr. W. A Slippy, Jr., for his able assistance with many of the technical problems of the experimental work. I also wish to thank Dr. D. H. Baldwin and Dr. W. H. Hart for their helpful and stimulating discussions.

Financial assistance for this investigation was received from the United States Atomic Energy Commission.

Finally, I wish to thank the Student Policies Committee of the University of Florida for its support in granting me a College of Engineering Fellowship.

TABLE OF CONTENTS

Page

ACKNOWLEDGEMENTS..... ii

LIST OF TABLES..... iv

LIST OF FIGURES..... v

ABSTRACT..... ix

INTRODUCTION..... 1

CHAPTER

I. PREVIOUS INVESTIGATIONS..... 3

II. EXPERIMENTAL METHODS AND PROCEDURES..... 13

III. EXPERIMENTAL RESULTS..... 27

IV. DISCUSSION..... 58

V. CONCLUSIONS..... 97

BIBLIOGRAPHY..... 99

BIOGRAPHICAL SKETCH..... 105

LIST OF TABLES

Table		Page
1	Composition of Arc-Melted Sponge Zirconium	14
2	Equilibrium Stress-Strain Measurements	56
3	Activation Volume Measurements	93

LIST OF FIGURES

Figure		Page
1.	Microstructure of the as-received zirconium. Magnification 150X. Polarized light.....	15
2.	Schematic representation of the rolling texture of polycrystalline zirconium plate. The basal-plate trace is indicated by a dashed line in each grain.....	17
3.	Completed tensile specimen with strain gages and lead wires attached. A specimen with no gages and an unmounted strain gage are also shown.....	21
4.	Schematic view of testing apparatus showing the rapid unloading device.....	24
5.	Photograph of constant temperature oil bath.....	25
6.	Microstructure of transverse zirconium specimen prestrained 0.2 per cent by tension at 77°K. Magnification 250X. Polarized illumination.....	28
7.	Microstructure of a transverse zirconium specimen prestrained 1.84 per cent by tension at 77°K. Magnification 250X. Polarized illumination.....	30
8.	Microstructure of a transverse zirconium specimen prestrained 3.84 per cent by tension at 77°K. Magnification 250X. Polarized illumination.....	31
9.	Typical two cycle room temperature tensile stress-strain diagram for a prestrained transverse zirconium specimen. (0.65 per cent prestrain at 77°K by rolling).....	32
10.	Fractional cyclic hysteresis energy absorption for transverse zirconium specimens as a function of tensile prestrain at 77°K.....	34

Figure Page

11. Fractional cyclic hysteresis energy absorption for prestrained zirconium specimens as a function of stress amplitude..... 36

12. Fractional cyclic hysteresis energy absorption for a prestrained zirconium specimen as a function of the test temperature..... 37

13. Fractional cyclic hysteresis energy absorption for a prestrained zirconium specimen as a function of tensile strain rate..... 38

14. The elastic aftereffect in a prestrained zirconium specimen stressed to 15,000 psi and quickly unloaded..... 39

15. The elastic aftereffect curves at various temperatures in a prestrained zirconium specimen prestrained 0.65 per cent by tension and stressed to 15,000 psi and quickly unloaded..... 41

16. Elastic aftereffect curves for a zirconium specimen prestrained 3.0 per cent by cold rolling at 77°K for temperatures between 40°C and 80°C..... 42

17. Elastic aftereffect curves for five zirconium specimens of varying prestrains tested at 80°C.. 43

18. Relationship between the unrelaxed modulus, relaxed modulus, and the stresses and strains as used in the following discussion..... 45

19. Near equilibrium stress-strain curve at 80°C for a zirconium specimen prestrained 0.65 by tension 46

20. Stress-strain curve recorded on tensile machine operating at a strain rate of 5×10^{-7} seconds^{-1} for the same specimen shown in Figure 19..... 47

21. Near equilibrium stress-strain curve at 80°C for a zirconium specimen prestrained 0.20 per cent by tension..... 50

22. Near equilibrium stress-strain curve at 80°C for a zirconium specimen prestrained 0.40 per cent by tension..... 51

23. Near equilibrium stress-strain curve at 80°C for a zirconium specimen prestrained 0.64 per cent by tension..... 52

Figure Page

24. Near equilibrium stress-strain curve at 80°C for a zirconium specimen prestrained 1.36 per cent by tension..... 53

25. Near equilibrium stress-strain curve at 80°C for a zirconium specimen prestrained 2.40 per cent by tension..... 54

26. Near equilibrium stress-strain curve at 80°C for a zirconium specimen prestrained 3.00 per cent by cold rolling..... 55

27. The relationship between the $\{11\bar{2}1\}$ plane and the "a" $<11\bar{2}0>$ slip dislocations in the zirconium hexagonal crystal structure. (a) $\{11\bar{2}1\}$ twin plane in hexagonal crystal. (b) Projection of $\{11\bar{2}1\}$ twin planes on basal plane showing their intersections with the a_1, a_2, and a_3 slip dislocations..... 64

28. (a) The relation between the $\{11\bar{2}1\}$ twin habit plane, the twinning dislocation (t) Burgers vector, and the unit $<11\bar{2}0>$ vector in the basal plane. (b) View along twin plane between twinned and untwinned crystal showing t Burgers vector dislocation..... 66

29. Two possible configurations for the growth of a twin terrace through non-moving dislocation poles. (a) Twin terrace moving from left to right. (b) Twin terrace moving from right to left..... 69

30. The line tension of a circular dislocation as a function of its radius of curvature..... 72

31. Schematic illustration of $\{11\bar{2}1\}$ twin interface showing (a) the probable dislocation distribution along the twin and in the adjoining grains and (b) the proposed model substituting a single dislocation at the twin edge..... 75

32. Measured surface area of $\{11\bar{2}1\}$ twins as a function of the amount of prestrain..... 77

33. Total relaxable or anelastic strain at 15,000 psi as a function of prestrain for zirconium specimens tested at 80°C..... 78

Figure Page

34. Comparison between the tensile near equilibrium and the 5 x 10^{-6} $second^{-1}$ strain rate stress-strain curves at 80°C for cyclically loaded zirconium specimen prestrained 0.65 per cent by tension at 77°K..... 82

35. Curves of ln tanh $\alpha\epsilon/2RT$ as a function of time for various values of α corresponding to the data obtained in Figure 15 at 40°C..... 88

36. Curves of ln tanh $\alpha\epsilon/2RT$ versus time for the elastic aftereffect at various temperatures of a zirconium specimen prestrained 0.65 per cent by tension. (Corresponding to Figure 15)..... 89

37. Curves of ln tanh $\alpha\epsilon/2RT$ versus time for the elastic aftereffect at various temperatures of a zirconium specimen prestrained 3.0 per cent by cold rolling. (Corresponding to Figure 16).. 90

38. Activation energy plot for the data of Figures 36 and 37..... 92

39. The tensile machine relaxation period for room temperature creep as a function of the reciprocal of the absolute temperature for longitudinal zirconium specimens..... 95

Abstract of Dissertation Presented to the Graduate Council in Partial Fulfillment of the Requirements for the Degree of Doctor of Philosophy

SOME ANELASTIC PROPERTIES OF ZIRCONIUM RESULTING FROM PRESTRAIN AT 77°K

By

Edward Philip Dahlberg

April 1967

Chairman: Dr. R. E. Reed-Hill
Major Department: Metallurgical and Materials Engineering

This study is concerned with the mechanical hysteresis and anelastic properties of polycrystalline zirconium which result from the reversible thermally activated motion of the boundaries of deformation twins. Straight rolled polycrystalline zirconium plate stock was prestrained at 77°K in order to nucleate numerous fine $\{11\bar{2}1\}$ twins in an otherwise almost undistorted matrix. Subsequent tensile deformation at elevated temperatures showed marked deviation from linear behavior in the stress-strain curves at an initial resolved shear stress of approximately 2,500 psi, which is at least ten times lower than the normal 0.2 per cent offset yield point for this material. The development of large anelastic strain at comparatively low stress levels indicates the ease with which $\{11\bar{2}1\}$ twin boundaries are able to move.

On cyclic loading at low frequencies in a tensile machine, large mechanical hysteresis energy losses were observed over the range of temperature from -72°C to 80°C. Comparative area measurements of the hysteresis loops

showed the energy losses were a sensitive function of the amount of prestrain and reached a maximum at approximately 0.65 per cent prestrain. The losses were stress amplitude dependent, increased with increased temperature, and decreased with increased strain rate or cycle frequency.

The rate of the development of the anelastic strain at constant stress on loading or its recovery on unloading was found to obey a relation of the type,

$$\epsilon = - \frac{RT}{a} \ln \tanh \frac{t + t_o}{2 \tau_\sigma}$$

The anelastic strain relaxation processes were found to be controlled by a single relaxation time which varied markedly with test temperature. An activation energy for these processes was found to be approximately 23,000 calories per mole and did not vary significantly over the range of temperature used in these experiments.

The study permitted the determination of the relaxed modulus and activation volume for twin boundary motion. The kinetics of the anelastic strain development indicate that twin boundary migration may be controlled by slip deformation. The stress concentrations at the tapered twin edges are thought to induce slip deformation in the adjoining matrix. As this deformation increases or decreases, the twin either thickens or thins accordingly. The correlation between the activation energy and the activation volume for twin boundary migration with that for low temperature creep in zirconium suggests such a controlling mechanism.

INTRODUCTION

The increased use of the metal zirconium for integral structural components in the construction of nuclear power reactors has created the need for a more complete understanding of its mechanical properties. Of particular interest and concern is the way in which zirconium in the form of a polycrystalline aggregate will respond to applied stresses at levels both above and below the macroscopic yield point. Because of their anisotropic crystal structures, the hexagonal metals such as zirconium generally have a restricted and unsymmetrical set of slip systems. It has been observed that deformation twinning often plays an important role in the plastic deformation of such anisotropic materials.

An intensive and continuing investigation of the nature of deformation twinning in zirconium has been carried out by Professor R. E. Reed-Hill and his co-workers at the University of Florida. This investigation has concerned the role of strain, strain rate, temperature, grain size, and grain orientation in the deformation processes. During the course of this investigation, it was observed that in zirconium specimens, oriented transversely with respect to the principal rolling direction of straight rolled plate, small

amounts of mechanical deformation at 77°K would nucleate numerous fine deformation twins in an otherwise almost undistorted matrix. The analysis of these deformed specimens showed that nearly all of the plastic flow at small strain levels of approximately 1 per cent could be accounted for by the shear associated with the mechanical twinning. The most significant form of twin was observed to be the $\{11\bar{2}1\}$ type.

An increase of nearly 50 per cent was observed in the room temperature elongation of transverse specimens of zirconium containing the low temperature nucleated twins. In addition, when cyclically loading these prestrained specimens in tension at room temperature, a large mechanical hysteresis and elastic aftereffect were evident in the stress-strain curves at stresses significantly below the macroscopic yield point. The magnitude of the energy absorbed during cyclic loading was approximately 25 per cent of the maximum tensile strain energy.

The research reported in this dissertation was undertaken with the aim of providing a clearer understanding of these mechanical hysteresis and elastic aftereffect phenomena. The experimental evidence presented deals with the relaxation associated with the small reversible and thermally activated motion of $\{11\bar{2}1\}$ type deformation twins in zirconium. These experimental results will be interpreted in terms of possible mechanisms for the twin boundary movements.

CHAPTER I

PREVIOUS INVESTIGATIONS

In view of the nature of the present investigation, it is desired to review previous research in three areas: the study of anelasticity in metals; anelasticity resulting from the motion of twin boundaries; and the mechanical deformation of pure zirconium. It is convenient to begin with a consideration of anelasticity.

Anelasticity in Metals

C. M. Zener, in his book Elasticity and Anelasticity of Metals (1)*, adopted the term anelasticity to describe those properties of solids where, in the pre-plastic range, stress is not uniquely related to strain. Mechanical hysteresis or internal friction, strain relaxation at constant stress, stress relaxation at constant strain, and changes in the elastic modulus with frequency of measurement are all aspects of anelasticity. Anelasticity in metals is commonly observed as time dependent or recoverable creep strain. At stresses generally below the critical shear stress for plastic yielding a

---

*Numbers in parentheses refer to entries in the bibliography.

by B. P. Haigh (5). Using a series of thermocouples attached to a cylindrical specimen subjected to equal values of push and pull loading, he was able to measure the temperature gradient in the metal and determine the rate of heat evolution during the cyclic loading. He observed that the thermal hysteresis increased with an increase in the range of stress but diminished during successive cycles within a given range of load. Changes in the value of the Young's modulus due to strain have been observed by W. Koster and K. Rosenthat in 1938 (6), and the elastic aftereffect in carbonyl iron was studied by V. G. Richter in 1938 (7).

By measuring the residual strain remaining in iron wires after twisting as a function of time at various temperatures, Richter was able to determine an activation energy which could be associated with the anelastic strain recovery process. He also pointed out the similarity in behavior between the mechanical aftereffect and the anomalous magnetic aftereffect in mild steel. Later, J. Snock (8) developed the theory of preferred atomic sites for carbon and nitrogen when the iron crystal lattice is subject to an applied stress. He pointed out that the application of a tensile stress along the <100> directions would induce a preferred equilibrium distribution of carbon and nitrogen in the interstitial sites along these directions. The additional numbers of interstitial atoms in the sites parallel to the applied stress permit the anelastic strain component to develop as thermal

activation assists in the redistribution of the carbon and nitrogen atoms.

More recent studies of the mechanical hysteresis of metals that occurs in the pre-macroscopic yield region of the stress-strain curves have been carried out on zinc by J. M. Roberts and N. Brown (9), on beryllium by W. Bonfield and C. H. Li (10), on magnesium by J. M. Roberts and D. E. Hartman (11), and on iron by N. Brown and K. F. Lukens (12), N. Brown and R. A. Ekvall (13), and P. Lukas and M. Klesnil (14). In part, these studies have been developed around the theory of dislocation damping presented by A. Granato and K. Lucke (15, 16). In this theory it is assumed that dislocations are pinned along their lengths by impurity atoms and also by dislocation network nodes. Under the action of a stress, the dislocations bow out between the impurity pinning points until at a critical strain they break away and bow out between the primary intersection nodes. These longer dislocation loops continue to bow out until the maximum stress is reached. In cyclic stressing, therefore, the mechanical hysteresis or internal friction can be divided into two distinct stages: one, amplitude independent internal friction where the dislocations vibrate between the impurity pinning points; and two, the amplitude dependent internal friction where the vibration is between the dislocation network nodes. The critical breakaway stress is that stress which separates these two stages and occurs when the dislocations are freed from their impurity atmospheres.

Also in the above mentioned studies, mechanical hysteresis and the nonlinear nature of the materials' stress-strain responses have been analyzed in terms of the movement of a restricted number of slip dislocations in certain grains forming dislocation pile-ups at the grain boundaries. The model for this type of analysis has been discussed by A. H. Cottrell (17). Under an applied stress a number of dislocations move over the slip plane to grain boundaries where they are stopped. The pile-ups of dislocations through a back stress reduce the applied stress at the dislocation source. An equilibrium condition is reached when the applied stress is reduced to zero by the back stress of the pile-up. When the dislocation motion is restricted by a frictional stress such as a Peierls stress, the motion can be thermally activated. In such a case the pile-up of dislocations at the grain boundary can be formed as a function of time. The number of dislocations in a pile-up which exist in equilibrium with an applied stress has also been treated by Cottrell (17). This number is

$$n = \frac{\pi L \sigma K}{\mu b}$$

where n equals the number of dislocations, L is the radius of the grain, K is a numerical factor approximately unity, μ is the shear modulus, and b the Bergers vector of the dislocations. Because of the friction stress, mechanical hysteresis and elastic aftereffect phenomena will be evident in the development of these dislocation pile-ups.

Anelasticity and Twin Boundary Movements

B. P. Haigh (18), in a discussion of a paper by B. Chalmers (19), first suggested that mechanical hysteresis and elastic aftereffect phenomena might be associated with the twinning and detwinning of metals. He felt that twinning and detwinning occurring in a cyclic process during successive variations of stress might be a probable cause of elastic hysteresis. Zener (1) pointed out that inhomogeneous regions in a metal, such as twins, might provide the necessary relaxation centers to produce these effects. Work by F. T. Worrell (20) and F. T. Worrell and A. V. Siefert (21) on the damping capacity of copper manganese alloys indicates that the energy loss is due to the stress induced motion of twin boundaries. Twins are readily formed in an 88 per cent manganese 12 per cent copper alloy quenched to room temperature from 925°C. The internal friction decreases together with the amount of twinning, observed by optical means, after annealing for various times at an intermediate temperature.

Mechanical hysteresis in the stress-strain curves of uranium was also ascribed to the motion of twin boundaries by E. R. W. Jones and W. Monro (22). They observed that the energy dissipated during cyclic loading of uranium was an order of magnitude greater than that in steel or brass samples

tested under the same loading conditions. They concluded that the large energy loss was due to mechanical twinning and detwinning. The stress induced motion of twin boundaries was shown to be responsible for deformation in AuCd β' and β" alloys by H. K. Birnbaum and T. A. Read (23). They proposed that the motion of the twin boundaries resulted from the addition of successive atomic planes to the twinned lattice by the homogeneous nucleation of twinning dislocation loops. An alternative mechanism which they proposed was the dissociation of a perfect dislocation into a twinning dislocation and a sessile pole dislocation. The theory of a pole mechanism (24, 25) for twin growth would account for the pile-up of dislocations at the outermost twin edges. The twinning dislocations would be thermally activated in moving out of a Peierls valley and would reduce the applied stress at the dislocation source. On unloading they would move back to the source due to the elastic constraints of the surrounding grains thus producing the mechanical hysteresis and elastic aftereffect phenomena.

The theoretical considerations for the relaxation of strain at constant stress and the relaxation of stress at constant strain have recently been presented by R. E. Reed-Hill and E. P. Dahlberg (26, 27). This analysis of the time dependence of internal friction effects connects the well-known exponential equation

$$\epsilon = \epsilon_o e^{-\frac{t}{\tau\sigma}}$$

where ϵ is the strain at any instant, ϵ_o is the maximum strain at zero time, and τ_σ is the relaxation time for constant stress, with the empirical relation

$$\epsilon = A \ln t + B,$$

where ϵ is the instantaneous strain, t is the time, and A and B are constants (28, 29). These two equations are related through the following two formulations:

$$\epsilon^* = -\frac{RT}{\alpha} \ln \tanh \frac{t + t_o}{2\tau_\sigma}$$

$$\tanh \frac{\alpha\epsilon^*}{2RT} = \tanh \frac{\alpha\epsilon_o}{2RT} e^{-\frac{t}{\tau\sigma}}$$

where ϵ^* is the total relaxable strain at any instant. The value of α in these derivations is related to the activation volume of the thermally activated relaxation processes through the relaxed and unrelaxed elastic moduli,

$$V = \frac{\alpha(M_u - M_r)}{\bar{m} M_u M_r}$$

where V is the activation volume, M_u is the unrelaxed modulus, M_r is the relaxed modulus, and $\bar{m}$ is an orientation factor.

Mechanical Deformation of Pure Zirconium

An extensive analysis of the slip and twinning deformation mechanisms in zirconium has been carried out recently by several investigators. E. J. Rapperport and C. S. Hartley (30) in studying the deformation of large zirconium single crystals, reported slip deformation on the prism planes, $\{10\bar{1}0\}$, at room temperature. J. L. Martin and R. E. Reed-Hill (31) observed that basal slip becomes an important secondary mode of deformation in the formation of kink bands at elevated temperatures in polycrystalline material. Additional slip deformation has been reported to occur on the $\{10\bar{1}1\}$ and $\{11\bar{2}2\}$ pyramidal planes by D. H. Baldwin and R. E. Reed-Hill (32) who worked with polycrystalline zirconium deformed in torsion.

Twins in single crystals of zirconium have been reported to occur on $\{10\bar{1}2\}$, $\{11\bar{2}1\}$, $\{11\bar{2}2\}$, and $\{11\bar{2}3\}$ by E. J. Rapperport (33, 34). The frequency of twinning was found to be greatest on the $\{11\bar{2}1\}$ planes (30). The existence of twins on the $\{10\bar{1}2\}$, $\{11\bar{2}1\}$, and $\{11\bar{2}2\}$ has been further verified in polycrystalline zirconium by Iu. N. Sokurskii and L. N. Protsenko (35), R. E. Reed-Hill, W. A. Slippy, Jr., and L. J. Buteau (36), and D. H. Baldwin and R. E. Reed-Hill (32).

The low temperature deformation characteristics in transverse polycrystalline zirconium tensile specimens have been investigated (37, 38, 39). Briefly, the results of

these studies show that twinning is the primary deformation mechanism at 77°K for strains of approximately 3 per cent. At these low temperatures three twinning systems have been observed in quantity, $\{10\bar{1}2\}$, $\{11\bar{2}1\}$, and $\{11\bar{2}2\}$. The volume fraction of twins of each particular type has been measured using quantitative metallographic techniques by R. E. Reed-Hill, E. R. Buchanan, and F. W. Caldwell, Jr. (40). Because of its high twinning shear (0.63) and large volume fraction at tensile strains of less than 3 per cent, nearly all of the deformation can be accounted for by $\{11\bar{2}1\}$ twins. With increasing amounts of strain the role of twinning decreases, and slip becomes the primary mode of plastic deformation. This shift is believed to result from lattice reorientation and nucleation of slip dislocations due to twinning.

Transverse specimens of polycrystalline plate zirconium which have been prestrained approximately 1 per cent at 77°K have a large number of grains containing deformation twins of the $\{11\bar{2}1\}$ type completely surrounded by a matrix of grains which are essentially undeformed. An additional strain component at more elevated temperatures should, therefore, result from the stress induced motion of the twin boundaries. The resulting twin boundary motion could be expected to be thermally activated and provide the mechanism for mechanical hysteresis and elastic aftereffect phenomena.

CHAPTER II

EXPERIMENTAL METHODS AND PROCEDURES

Material

The material used in this investigation was arc-melted sponge zirconium which had been straightaway rolled into 1/2-in.-thick plate. It was purchased from the Wah Chang Corporation of Oregon and was designated heat number 4-56-1367 Zr (41). The Wah Chang heat analysis for this material is presented in Table 1.

Figure 1 shows the microstructure of the as-received zirconium at a magnification of 150X using polarized light. The plane of the micrograph is normal to the principal rolling direction of the as-received plate. As can be seen from the figure, the material has a fairly well-developed duplex grain structure with both large and small grains appearing in the two-dimensional plane of the polish. The average grain diameter was determined to be 3×10^{-3} centimeters by the linear intercept method. This corresponds to an ASTM grain size number of approximately 4.

The rolling texture of a similar heat of polycrystalline plate zirconium has been verified by an extensive analysis of the distribution of basal plane traces in relation to the

TABLE 1

COMPOSITION OF ARC-MELTED SPONGE ZIRCONIUM

Element	Composition (parts per million)	Element	Composition (parts per million)
Sn	< 10	Mg	< 10
Cr	< 10	Mn	< 10
Fe	435	Mo	< 10
Ni	10	N	39
Al	44	O	965
B	< 0.2	Pb	< 5
C	110	Si	71
Cd	< 0.3	Ti	< 20
Co	< 5	V	< 5
Cu	25	W	30
Hf	< 40	Zn	< 50

Balance Zirconium

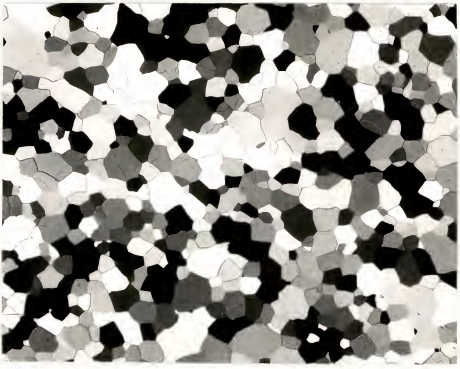

Figure 1. Microstructure of the as-received zirconium. Magnification 150X. Polarized light.

principal rolling direction (42). It was determined in these investigations that the basal planes of almost all the grains lie parallel or nearly parallel to the principal rolling direction in the plate. This texture is illustrated in Figure 2. It is roughly equivalent to a wire texture and is fairly common in commercially available plate zirconium. The basal plane normals are uniformly distributed in space about the rolling direction axis. Longitudinal tensile specimens, cut with the tensile axis parallel to the rolling direction, deform for the most part by slip since the stress is applied parallel to the basal planes in nearly all of the grains. In this orientation the resolved shear stress for slip on the pyramidal and prism planes is high. In transverse tensile specimens, cut with the tensile axis parallel to the long transverse plate direction, however, a large fraction of the grains are oriented so their basal planes are normal to the stress axis. In this orientation these grains have slip directions normal to the tensile stress axis and cannot deform easily by slip. In transverse tensile specimens, therefore, twinning becomes important as a mode of plastic deformation.

Specimen Preparation

Standard 1/8-in. diameter tensile specimens of the same general form as that described by P. L. Rittenhouse and M. L. Picklesimer (43) were machined from the 1/2-in. zirconium plate stock in the transverse orientation. Pieces

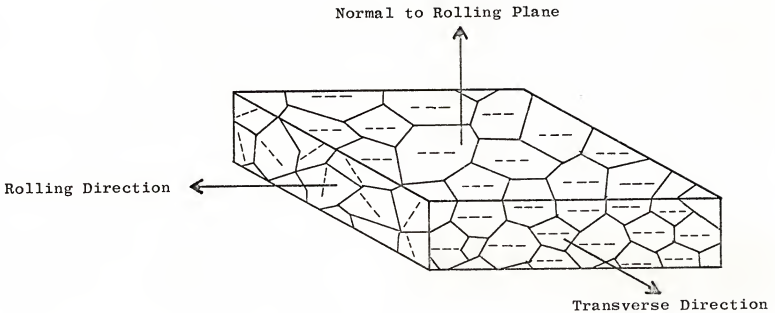

Figure 2. Schematic representation of the rolling texture of polycrystalline zirconium plate. The basal-plane trace is indicated by a dashed line in each grain.

1/2 x 1/2 x 3 1/2 inches were cut from the plate using a metal cutting band saw. Each rough cut blank was marked so that the position of the rolling plane normal could easily be identified on the completed specimen. The rectangular pieces were rough machined on a lathe into tensile blanks 3 inches long. The specimens had 1/2-in.-lengths of 1/4-20 threads at either end. The gage section was reduced in this operation to 3/16 of an inch.

Final reduction of the gage section to an approximate diameter of 0.130 inch was performed by a chemical acid machining operation. The acid machining was done in a solution of 45 parts ' water, 45 parts ' nitric acid, and 10 parts ' hydrofluoric acid (44). The threaded ends of each specimen were dipped in molten paraffin for protection during acid machining. The chemical machining was done in stages with reapplication of the paraffin coating to prevent any undercutting by the acid solution at the ends of the reduced gage section. The final gage length was approximately 1 1/4 inches. The specimen diameter normally varied less than 0.002 inch along the gage length and were out-of-round by less than 1 per cent. All specimen diameters and gage lengths were measured using an optical comparator. These measurements were accurate to about 0.0002 inch.

Prestraining Techniques

The low temperature prestrain performed on the specimens used in this investigation was done either by cold rolling or by tensile deformation. In the first case the rough sawed blanks (1/2 x 1/2 x 3 1/2 inches) were soaked in liquid nitrogen and rolled lengthwise along the long transverse plate direction using a two high 6-in. Fenn rolling mill. The reduction in thickness per pass was kept small, and intermediate periods of soaking at 77°K insured that the rolling deformation took place near the liquid nitrogen temperature. After a predetermined reduction the blanks were machined to tensile specimens in the standard fashion.

Tensile prestraining was carried out on finished machined tensile specimens using a floor model Instron tensile machine. The crosshead of the Instron was operated at a rate of 0.002 inches per minute which produced a strain rate of approximately 5×10^{-5} seconds^{-1} in the 1 1/4-in.-gage length. The specimen was immersed in a Dewar flask of liquid nitrogen during the prestraining operation. Final strain percentages were determined by measuring the increased length of each specimen.

Microstrain Measurement Techniques

After the low temperature prestrain treatment each tensile specimen was prepared for microstrain measurements by attaching two wire resistance SR-4 strain gages along its

length. Two strain gage sizes were used during the course of these experiments; one, 1/4-in. long and the other, 1/2-in. long. Both gage types were epoxy backed temperature compensating gages approximately 0.2-in. wide. The strain gages were attached to the zirconium specimens with Eastman 910 adhesive and catalyst. The acid machined finish of the specimens was roughened by lightly rubbing 600-grit metallography paper over the gage lengths to insure proper adhesion of the strain gages. The specimens were washed in benzene, acetone, and finally, distilled water to remove any grease and other unwanted surface films. A thin uniform layer of adhesive was applied to the specimen in order to produce the most accurate strain measurements (45). The adhesive catalyst was applied to the underside of the strain gage. Care was taken to align the gages parallel to the tensile axis. While each gage wrapped nearly halfway around the specimen circumference, in all cases they were centrally located on the portion of the specimen corresponding to the original rolling plane.

Enameled copper lead wires one foot long were soldered to the strain gage tips. The entire gage assembly was then cleaned to remove any excess solder rosin and coated with a protective covering of a heat-curing silicone phenolic lacquer. This coating was cured in three stages, 15 minutes in air, 15 minutes at 50°C, and 1 hour at 90°C. Figure 3 shows a photograph of a completed tensile specimen with the strain gages and lead wires attached.

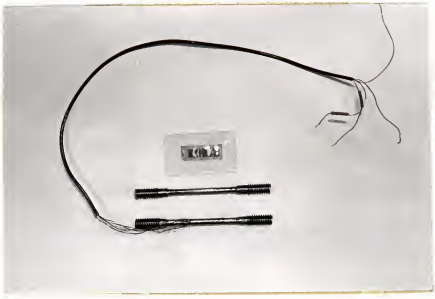

Figure 3. Completed tensile specimen with strain gages and lead wires attached. A specimen with no gages and an unmounted strain gage are also shown.

Testing Procedures

Tensile stress-strain mechanical hysteresis tests were performed on a standard floor model Instron tensile machine. The test specimen and a temperature compensation dummy specimen were immersed in a constant temperature oil bath mounted on the crosshead of the tensile machine. The strain gages of the two specimens were attached in a four arm bridge configuration to the X-Y recorder chart drive of the Instron machine. The X-Y recorder gave a record of load versus specimen strain. A variable resistor was used to calibrate the strain displacement of the X-Y recorder. This resistor was calibrated with a standard SR-4 strain indicator to provide a strain indication of 500-microinches per inch for each individual specimen when placed across an active arm of the strain gage bridge. The load indication of the recorder was calibrated in the usual way by hanging a fixed weight from the load cell of the Instron machine.

Tests were carried out at temperatures between room temperature and 80°C. The temperature controller could maintain the temperature of the oil bath to within 0.05°C of any preset temperature in this range. The bath temperature was measured using a thermometer reading in units of 0.1°C A 2-in.-diameter copper cylinder was placed around the test specimen and the temperature compensation dummy specimen in order to isolate them from any thermal fluctuations arising from currents set up by the stirring rod of the constant

temperature oil bath apparatus. No significant temperature gradient existed along the specimen length.

Strain rates were varied between the range of 5×10^{-4} and 5×10^{-6} seconds^{-1} corresponding to crosshead speeds on the Instron tensile machine of 0.2 inches per minute and 0.002 inches per minute. At faster strain rates the chart recorder of the X-Y drive system could not respond adequately to the microstrain changes in the specimen.

Strain relaxation tests at constant stress including anelastic aftereffect experiments were carried out utilizing the load weighing system of the Instron. In these tests the specimen strain was measured as a function of time using a standard SR-4 strain gage indicator. In the elastic after-effect tests the specimen was loaded to a maximum load, usually 200 pounds, then quickly unloaded to zero. A device permitting rapid unloading was inserted in the tensile machine between the upper loading pin and the specimen. A schematic view of the testing apparatus together with this unloading device is shown in Figure 4.

Elastic aftereffect as well as strain relaxation tests at constant non-zero stresses were performed on a modified creep rupture apparatus. This machine had a 40:1 lever arm in the loading system. Stress levels were maintained with several 1/2 lb weights loaded manually to the load pan. In order to minimize bending effects in this machine, a universal joint was inserted below the specimen. Figure 5 shows the experimental apparatus arrangement for these tests. The same constant temperature oil bath was used with this machine.

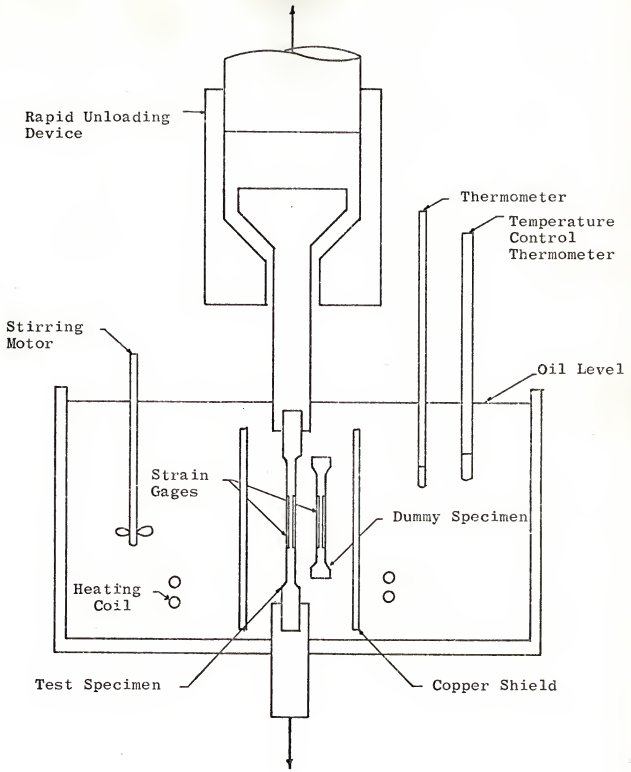

Figure 4. Schematic view of testing apparatus showing the rapid unloading device.

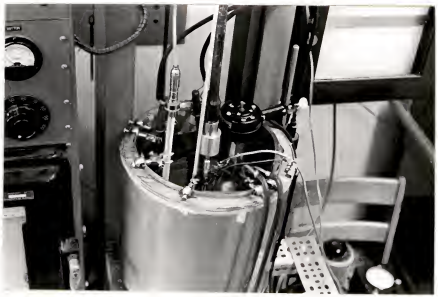

Figure 5. Photograph of constant temperature oil bath.

Hysteresis Area Measurements

Comparative area measurements of the mechanical hysteresis loops associated with the stress-strain curves recorded in this investigation were made using a self-compensating calibrated planimeter. The average values of three individual measurements for each area was used in reporting these results.

CHAPTER III

EXPERIMENTAL RESULTS

The experimental data obtained during the course of this investigation are presented, for the most part, in graphic form in the following chapter. Several $\{11\bar{2}1\}$ type twins were observed to nucleate when plate zirconium was prestrained at 77°K in the transverse orientation. These twins acted as relaxation centers to give a pronounced mechanical hysteresis and elastic aftereffect on subsequent testing at temperatures ranging between 0°C and 80°C. The magnitude of the mechanical hysteresis was measured as a function of temperature, strain rate, and amount of prestrain. The kinetics of the elastic aftereffect were determined as a function of temperature and amount of prestrain. The relaxed and unrelaxed moduli were measured as a function of the amount of prestrain at a constant temperature of 80°C. Finally, the critical stress at which significant amounts of anelastic strain developed for near equilibrium stress-strain tests was determined for specimens varying in amount of prestrain.

Microstructure of Prestrained Zirconium

Figure 6 shows the microstructure of a transverse specimen of zirconium which had been prestrained 0.2 per cent by

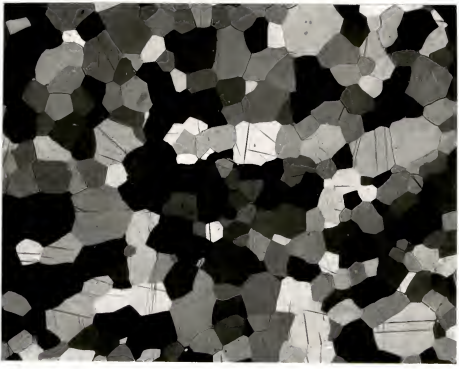

Figure 6. Microstructure of transverse zirconium specimen prestrained 0.2 per cent by tension at 77°K. Magnification 250X. Polarized illumination.

tension at 77°K. The plane of the photograph is normal to the principal rolling direction of the original plate material. The picture was taken on a Bausch and Lomb research metallograph using polarized light illumination at a magnification of 250. As can be seen from the micrograph, at this magnitude of strain the number of grains containing twins is very small. The number of twins per twinned grain is also small, and in many grains only a single twin can be seen. In addition, in a large number of the twinned grains only a single twin orientation is observed.

Figures 7 and 8 show the twin structure developed in specimens prestrained 1.84 per cent and 3.84 per cent by tension at 77°K. It can be seen in these micrographs that as the amount of strain at 77°K increases, the number of grains containing twins increases significantly. In addition, the number of twins in each twinned grain increases. Twins on several intersecting twin planes can also be observed in many of the grains in these more highly strained specimens.

Mechanical Hysteresis

The nucleation of twins in transverse specimens by prestrain at 77°K was observed to impart a large mechanical hysteresis to the material when subsequently tested in cyclic loading at room temperature. Figure 9 shows a typical hysteresis loop associated with the stress-strain curve of a zirconium specimen prestrained 0.65 per cent by cold rolling. The maximum stress in each cycle of loading was 14,500 psi

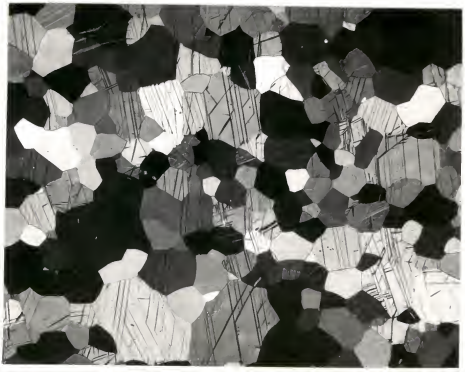

Figure 7. Microstructure of a transverse zirconium specimen prestrained 1.84 per cent by tension at 77°K. Magnification 250X. Polarized illumination.

Figure 8. Microstructure of a transverse zirconium specimen prestrained 3.84 per cent by tension at 77°K. Magnification 250X. Polarized illumination.

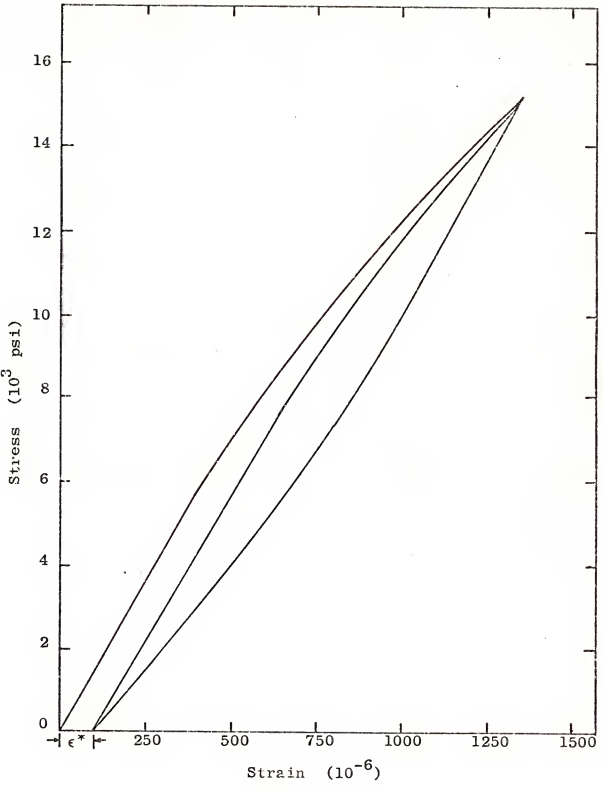

Figure 9. Typical two cycle room temperature tensile stress-strain diagram for a prestrained transverse zirconium specimen. (0.65 per cent prestrain at 77°K by rolling)

which is less than one half of the tensile yield stress for zirconium in this orientation. A significant deviation from the linear relation between stress and strain occurs at a stress of approximately 5,000 psi. Therefore, one would not expect to observe a mechanical hysteresis loop in tests run to maximum stresses below this level.

The magnitude of the energy absorbed during the cyclic loading of this specimen was approximately 26 per cent of the total tensile strain energy. In subsequent cycles this figure was reduced, but it remained constant after five cycles at about 18 per cent. That this energy loss is significant can be realized by comparing these results with similar tests of grey cast iron. In the latter the hysteresis losses are less than one third of those for the zirconium.

By testing specimens prestrained to various amounts, it was observed that the magnitude of the hysteresis loss reached a maximum at relatively small prestrain levels. Figure 10 shows the percentage of energy loss, the area of the hysteresis loop divided by the total area beneath the second loading curve on the stress-strain diagram, versus the amount of prestrain at 77°K for specimens prestrained in tension. The maximum cyclic energy absorption is seen to occur at a prestrain of slightly less than 1.0 per cent. Specimens without prestrain exhibit almost no mechanical hysteresis as is evident from Figure 10. Longitudinal specimens which deform primarily by slip when prestrained at 77°K also do not show a measurable hysteresis energy loss.

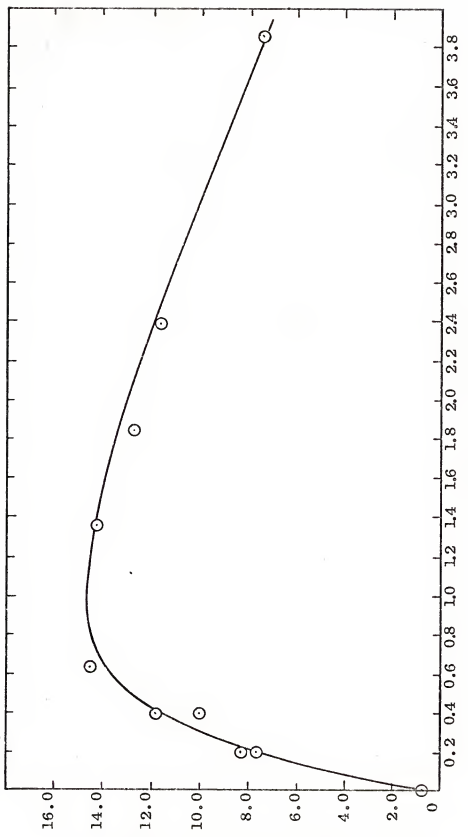

Figure 10. Fractional cyclic hysteresis energy absorption for transverse zirconium specimens as a function of tensile prestrain at 77°K.

The magnitude of the mechanical hysteresis energy losses was observed to be a sensitive function of the maximum stress amplitude. Figure 11 shows the room temperature cyclic energy loss as a function of stress amplitude for three specimens prestrained 0.2 per cent, 0.64 per cent, and 2.4 per cent by tension. It is again evident from this figure that the maximum hysteresis effects are associated with prestrains of less than 1.0 per cent. The curves have been extrapolated (dashed lines) back to a stress of 5,000 psi where the first deviation from linear behavior is observed on the stress-strain curves.

The hysteresis loop size was also found to be sensitive to the test temperature and strain rate. Figure 12 shows the percentage of cyclic energy absorbed in testing a specimen with 0.65 per cent tensile prestrain to a maximum stress of 15,000 psi at various temperatures from -72°C to 80°C. The per cent of energy absorbed as a function of strain rate for the same specimen tested at room temperature is shown in Figure 13.

Elastic Aftereffect

Another important aspect of the stress-strain curve shown in Figure 9 is the residual strain ϵ^* which remains in the specimen after one complete load and unload stress cycle. This residual strain diminishes to zero with time producing the elastic aftereffect phenomena. Figure 14 shows a simple elastic aftereffect curve at room temperature for a specimen

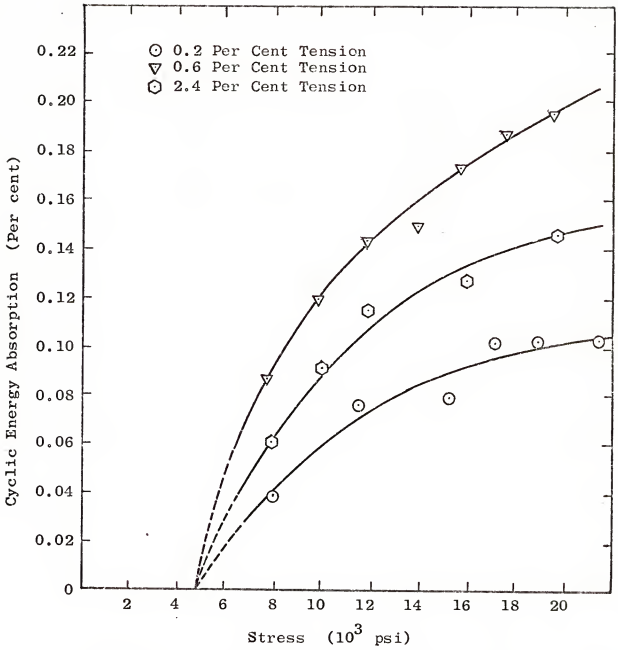

Figure 11. Fractional cyclic hysteresis energy absorption for prestrained zirconium specimens as a function of stress amplitude.

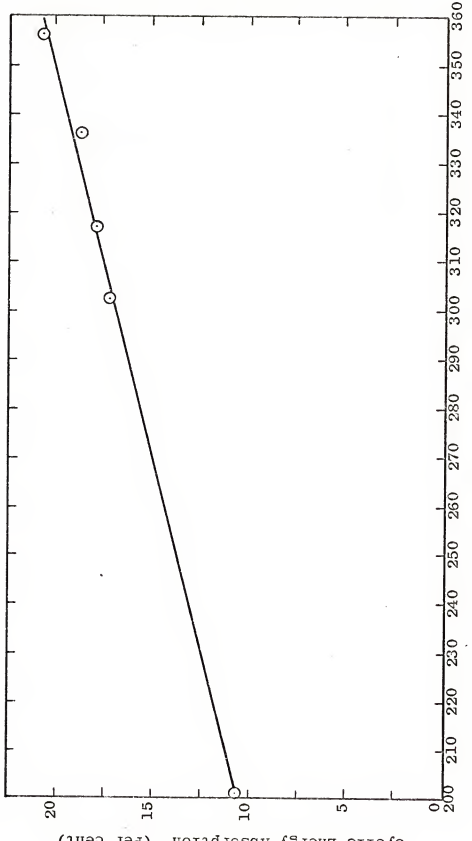

Figure 12. Fractional cyclic hysteresis energy absorption for a prestrained zirconium specimen as a function of the test temperature.

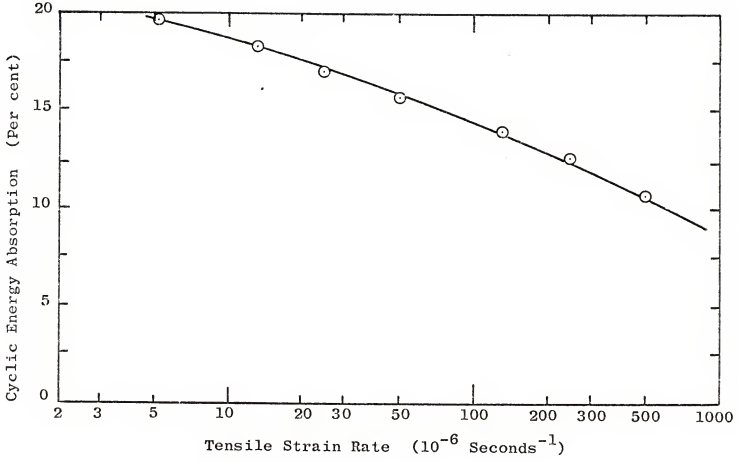

Figure 13. Fractional cyclic hysteresis energy absorption for a prestrained zirconium specimen as a function of tensile strain rate.

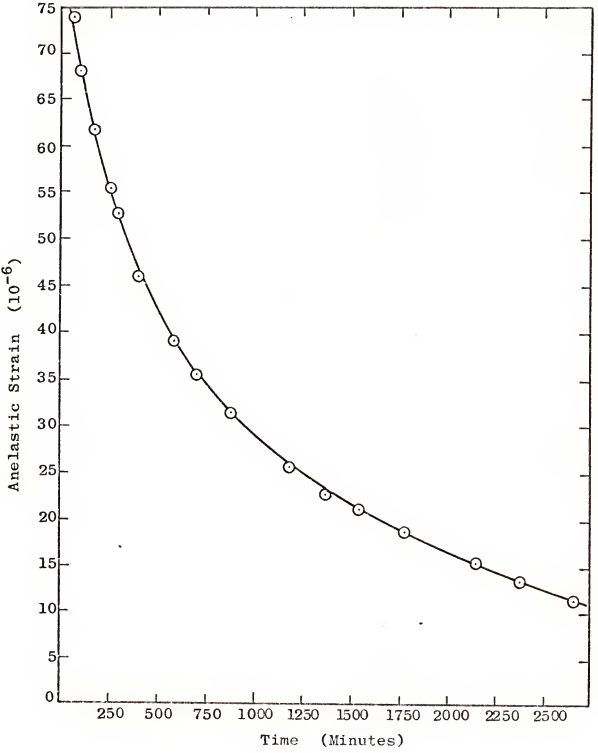

Figure 14. The elastic aftereffect in a prestrained zirconium specimen stressed to 15,000 psi and quickly unloaded.

prestrained 1.36 per cent by tension at 77°K. The specimen was loaded to a maximum stress of 15,000 psi and quickly unloaded to zero stress in less than two seconds. The residual strain was then measured as a function of time. As can be seen from this figure, the recovery process is relatively slow at this temperature and several days are required for the residual strain to reach zero.

At elevated temperatures the recovery process is much faster and nearly complete recovery of the residual strain is reached in a matter of minutes. Figures 15 and 16 show the recovery kinetics for specimens tested at various temperatures. The specimens were prestrained 0.65 per cent by tension and 3.0 per cent by cold rolling respectively. The aftereffect curves are drawn for test temperatures of 40°, 50°, 60°, 70°, and 80°C. Figure 17 shows the anelastic aftereffect recovery curves for five specimens of various prestrains tested at 80°C. As can be seen by this figure, the recovery kinetics for the aftereffect phenomena at this temperature do not vary markedly with changes in the amount of low temperature prestrain.

Relaxed Modulus

In the region of linear stress-strain response in a material where no anelasticity is present or in the instantaneous response of an anelastic material, the ratio of stress to strain is equal to the unrelaxed modulus. On the other hand, under constant load when the anelastic strain is

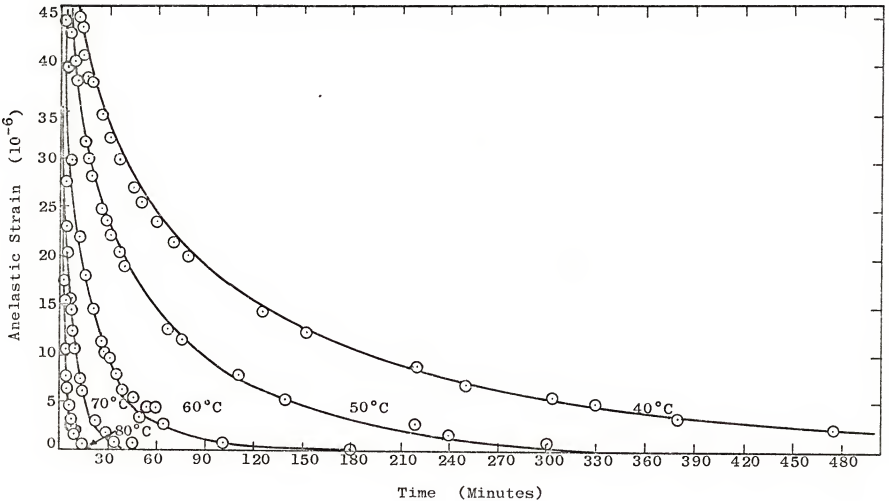

Figure 15. The elastic aftereffect curves at various temperatures in a prestrained zirconium specimen prestrained 0.65 per cent by tension and stressed to 15,000 psi and quickly unloaded.

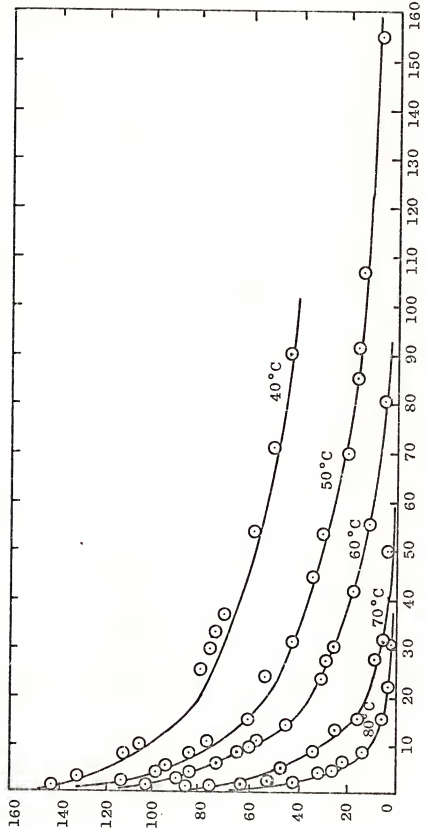

Figure 16. Elastic aftereffect curves for a zirconium specimen prestrained 3.0 per cent by cold rolling at 77°K for temperatures between 40°C and 80°C.

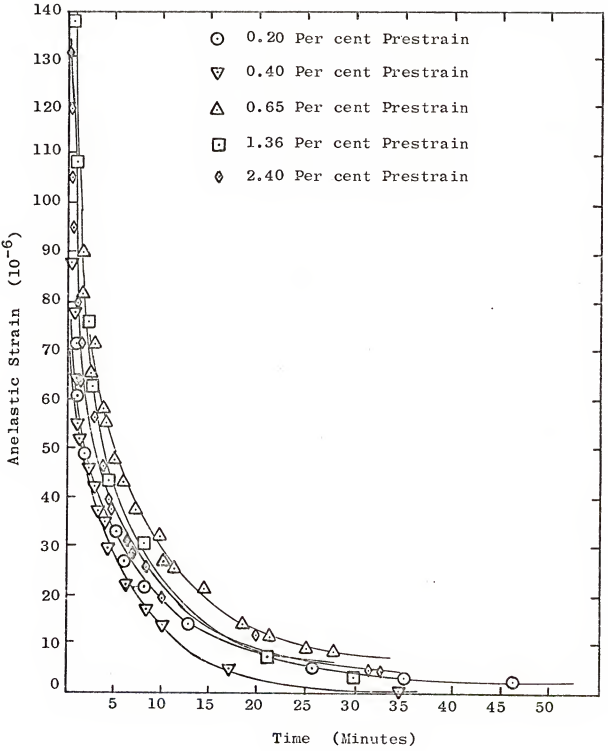

Figure 17. Elastic aftereffect curves for five zirconium specimens of varying prestrains tested at 80°C.

permitted to fully develop after a long period of time, the ratio of stress to equilibrium strain is the relaxed modulus. Figure 18 shows the relationship between the unrelaxed modulus, the relaxed modulus, the elastic strain, and the anelastic strain. A stress-strain curve for near equilibrium conditions for a zirconium specimen prestrained 0.65 per cent by cold rolling is shown in Figure 19. The temperature of the test in this instance was 80°C. The stress-strain diagram was obtained by loading the tensile specimen with 20-lb weights under dead loading conditions. Each loading weight corresponded to a tensile stress on the specimen of approximately 1,500 psi. The strain was measured with a standard SR-4 strain indicator. After a time sufficient to reach an approximate equilibrium condition in the specimen, usually 60 minutes at 80°C, an additional weight was added to the load. The strain relaxation process was then repeated at the higher stress level. The maximum stress applied to the specimen was approximately 15,000 psi. The specimen was then step unloaded in the same manner, and strain recovery measurements were made as the specimen length shortened at each lighter load. Figure 20 shows a similar stress-strain diagram obtained from loading a specimen in the Instron tensile machine at an extremely slow strain rate. The crosshead motion in this instance was 0.0002 inches per minute corresponding to a strain rate in the specimen of approximately 5×10^{-7} seconds^{-1}. One complete load and unload stress-strain cycle took 122 minutes to complete. By comparing

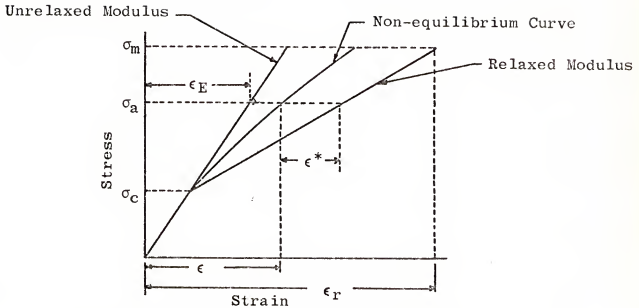

σ_a = applied tensile stress at any instant

σ_m = maximum tensile stress

σ_c = critical tensile stress for anelastic strain development

ϵ = total strain at any instant

ϵ_r = total relaxed strain, elastic plus anelastic

$\epsilon^* = (\epsilon_r - \epsilon)$ = relaxable strain at any instant

ϵ_E = elastic strain

Figure 18. Relationship between the unrelaxed modulus, relaxed modulus, and the stresses and strains as used in the following discussion.

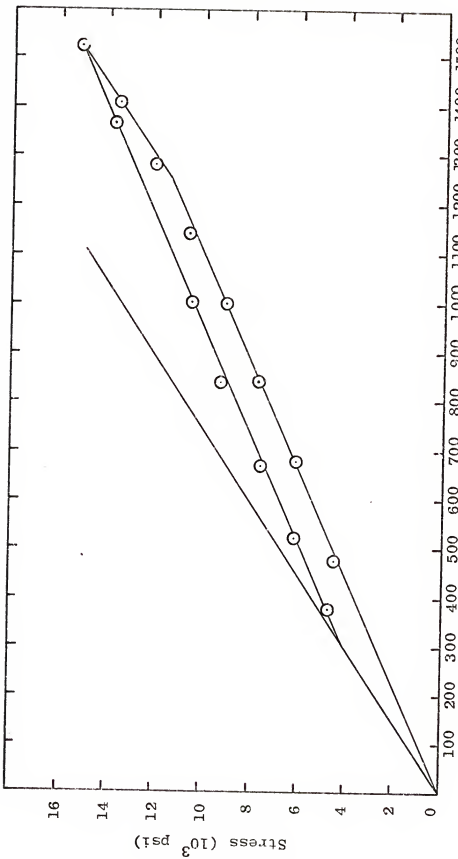

Figure 19. Near equilibrium stress-strain curve at 80°C for a zirconium specimen prestrained 0.65 per cent by tension.

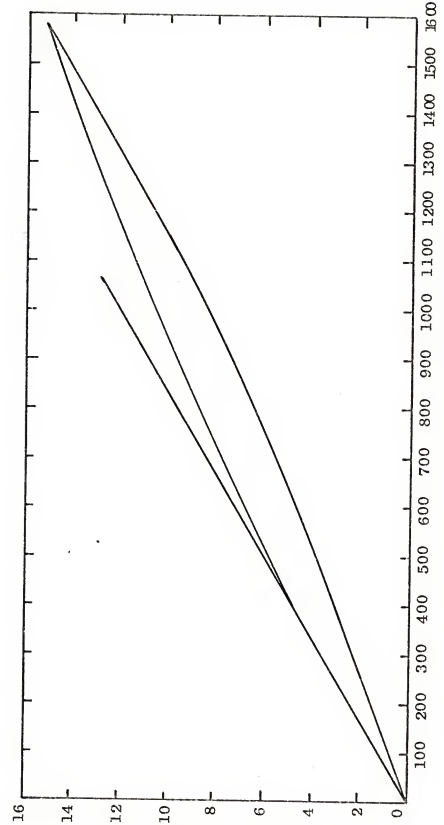

Figure 20. Stress-strain curve recorded on tensile machine operating at a strain rate of 5×10^{-4} seconds^{-1} for the same specimen shown in Figure 19.

Figures 19 and 20, it is evident that the equilibrium state was nearly reached at each point of the dynamic loading test.

Several significant results from the near equilibrium strain relaxation type test should be noted. Under stress-strain testing conditions, a relatively large mechanical hysteresis energy absorption loop exists. The magnitude of the energy absorption was approximately 15 per cent for the specimen shown in Figures 19 and 20. Normally, when the strain is allowed to relax sufficiently to maintain near equilibrium conditions, as in a torsion pendulum test run at a very low frequency or very high temperature, a material can be expected to respond along the relaxed modulus under both the load and unload segments of the test cycle resulting in no energy absorption or hysteresis loop. In this test, as is evident in both Figures 19 and 20, no anelastic strain was observed until a critical tensile stress of approximately 5,000 psi was reached. Similarly, on unloading, the unrelaxed modulus was followed with no anelastic strain recovery until after a critical unloading stress was passed.

After exceeding the critical stresses for the development or recovery of anelastic strain both on loading and unloading, the amount of strain was observed to be linearly related to the stress. The results show that this zirconium specimen had a clearly defined relaxed modulus. At this temperature the magnitude of the relaxed modulus was found to be 9.1×10^{-6} psi for this specimen.

Similar near equilibrium stress-strain curves at 80°C for specimens of various increasing prestrains are shown in Figures 21 through 26. It is evident from these figures that the basic stress-strain response of the material under these nearly equilibrium test conditions is the same for each of the prestrain treatments. A critical stress must be reached before anelastic strain relaxation appears both on loading and unloading. A sizable mechanical hysteresis energy absorption occurs even at near equilibrium conditions. In some cases of testing the strain remaining in the test specimen after unloading did not reach zero even after several hours at zero stress. The per cent strain remaining in the most severe case did not exceed 5 per cent of the total strain, elastic plus anelastic, measured at the maximum load. In these cases it was believed that some plastic strain component appeared due to creep when the specimen was subjected to high stresses during the extended period under load. The test of the zirconium specimen prestrained 0.4 per cent by tension showed the most significant amount of plastic strain. This specimen test was rerun using a fully automated strain sensing recorder in place of the SR-4 strain indicator. In this second test the near equilibrium stress-strain curve shown in Figure 21 was reproduced with no additional plastic, nonrecoverable strain component.

Table 2 lists the values for the relaxed and unrelaxed moduli together with the values of the critical stresses for anelastic strain development and recovery for the several

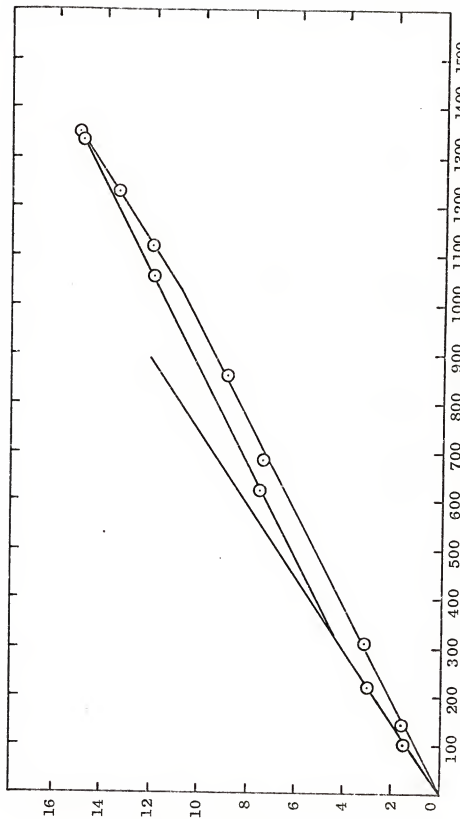

Figure 21. Near equilibrium stress-strain curve at 80°C for a zirconium specimen prestrainced 0.20 per cent by tension.

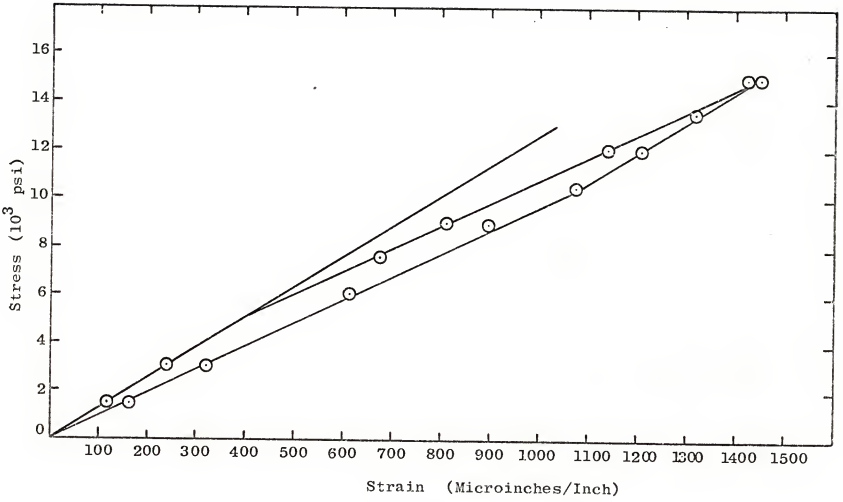

Figure 22. Near equilibrium stress-strain curve at 80°C for a zirconium specimen prestrained 0.40 per cent by tension.

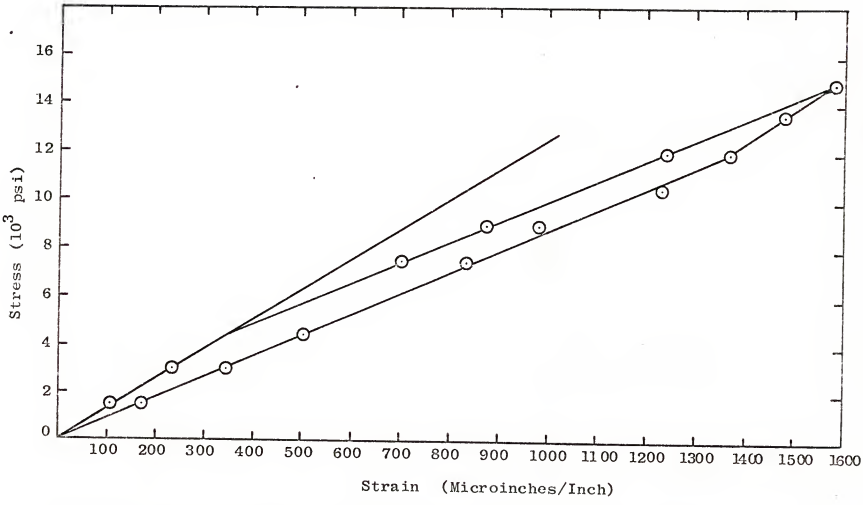

Figure 23. Near equilibrium stress-strain curve at 80°C for a zirconium specimen prestrained 0.64 per cent by tension.

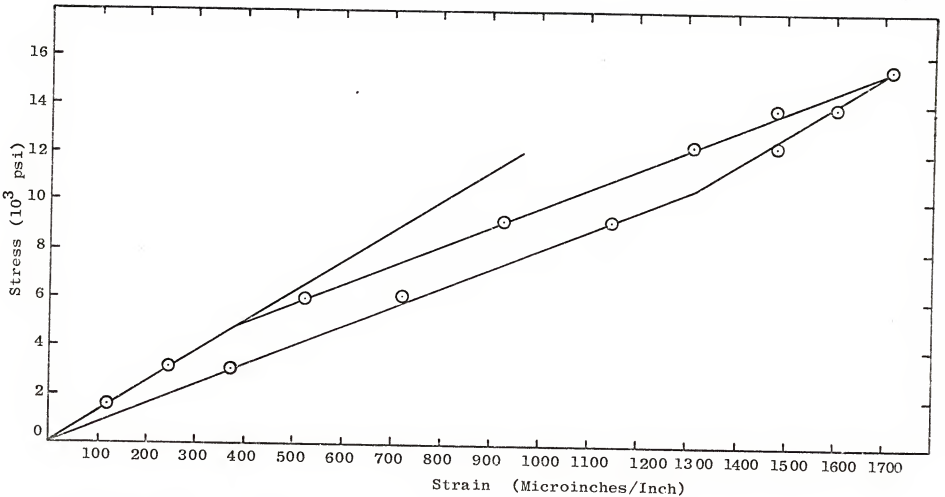

Figure 24. Near equilibrium stress-strain curve at 80°C for a zirconium specimen prestrained 1.36 per cent by tension.

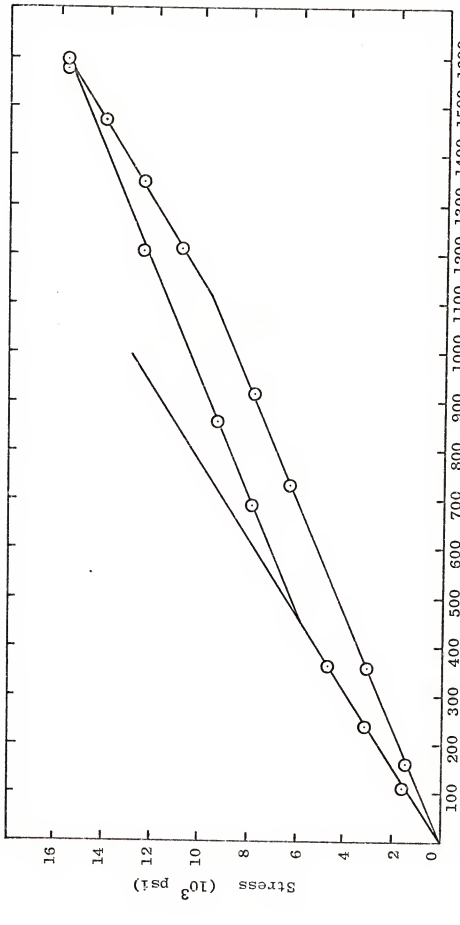

Figure 25. Near equilibrium stress-strain curve at 80°C for a zirconium specimen prestrained 2.40 per cent by tension.

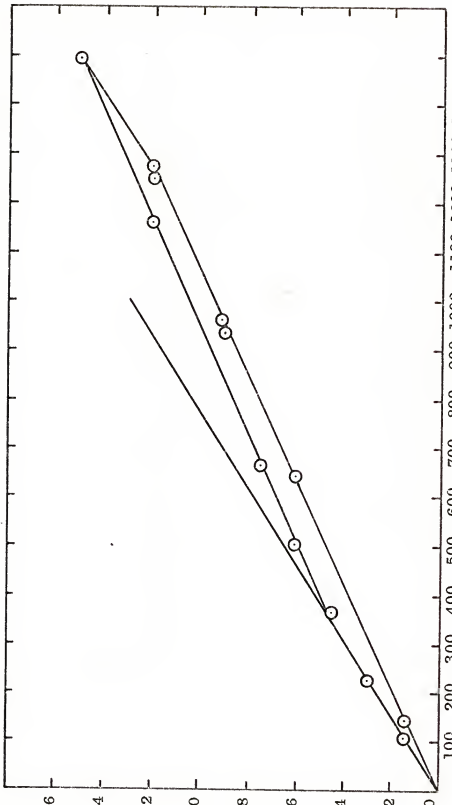

Figure 26. Near equilibrium stress-strain curve at 80°C for a zirconium specimen prestrained 3.00 per cent by cold rolling.

TABLE 2

EQUILIBRIUM STRESS-STRAIN MEASUREMENTS

Prestrain (per cent)	Unrelaxed Modulus (10^6 psi)	Relaxed Modulus (10^6 psi)	Maximum Anelastic Strain (10^6 psi)	Maximum Tensile Stress (psi)	Critical Tensile Stress-Loading (psi)	Critical Tensile Stress-Unloading (psi)
0.2 T	13.0	10.6	200	15,100	4,700	4,300
0.4 T	12.3	9.9	200	15,000	4,900	4,700
0.64 T	13.4	8.8	470	15,000	4,400	3,500
1.36 T	12.5	8.0	490	15,500	5,000	5,200
2.4 T	13.1	8.8	380	15,800	5,900	6,200
0.65 CR	13.5	9.1	400	15,100	4,300	4,000
3.0 CR	12.8	9.5	330	15,100	4,400	3,400

T = Tension Prestrain

CR = Cold Rolling Prestrain

specimens tested at 80°C and shown in Figures 18 through 25. The critical tensile stress for anelastic strain recovery is the maximum applied stress minus the stress at which significant strain recovery is observed on unloading.

CHAPTER IV

DISCUSSION

Twin Dislocation Intersection and Growth

It is generally agreed that an annealed metal crystal usually contains a well-defined Frank network of dislocations (46). The dislocations within the crystal form a metastable equilibrium arrangement in which the free energy of the crystal is minimized. The most common arrangement is for the dislocations to form in stable two-dimensional arrays at subgrain boundaries with a number of dislocations forming a three-dimensional network distributed in the interior of the subgrains. The Frank network is composed of a mechanically stable arrangement of dislocations connected at immobile nodes.

Such a network was observed in zirconium by J. E. Bailey (47, 48). Using techniques of thin film electron microscopy, he analyzed the dislocation arrangements in polycrystalline zirconium of two different compositions. He observed that in argon-arc-melted crystal bar zirconium, which contained approximately 0.03 weight per cent oxygen plus nitrogen, the dislocations formed complex tangles much like those observed in face-centered cubic metals. On the other hand, commercial

grade zirconium containing about 0.1 weight per cent of oxygen and nitrogen showed dislocations confined to specific crystal planes corresponding to slip operating on $\langle 10\bar{1}0 \rangle$ planes. In well-annealed samples of the commercial zirconium, moreover, dislocation networks were observed which were analyzed as networks on the basal plane.

The zirconium used in the present investigation was of the same approximate purity as the commercially pure material used by Bailey. It contained 960 parts per million of oxygen and 39 parts per million of nitrogen which compared very well with the 0.1 weight per cent of these gases in the material used by Bailey. On the basis of his microscopy work one could, therefore, conclude that the zirconium used in this study contained a well-defined Frank network of dislocations in the interior of the crystal grains. It is also interesting to note at this point that Bailey observed a pile-up of dislocations at a grain boundary in a sample of the commercial purity zirconium which had been deformed 1 per cent in tension.

The density of the grown-in dislocations that are found in the Frank network has been measured in both single crystals and polycrystalline material by several investigators. Many experimental methods are used to measure dislocation densities ranging from dislocation etch pit counts on the crystal surfaces, or direct observation in thin foils by electron microscopy, to deductions from X-ray misorientation measurements. In recent work on single crystals of well-annealed

pure iron, the dislocation density was determined by A. S. Keh (49) to be approximately 10^8 lines per square centimeter. P. B. Hirsch and J. S. Lally (50) determined a similar density of 10^8 lines per square centimeter in single crystals of magnesium. It would be expected that polycrystalline material would have a higher density than single crystals. J. E. Bailey (51) has presented some results from which the dislocation density in polycrystalline zirconium can be estimated. In an electron micrograph of an annealed zirconium specimen foil, the dislocation structure was detailed by the formation of a hydride precipitate on the foil surface at the points of emergence of the dislocations. By assuming a dislocation exists at each precipitate particle, even where contrast effects might not be favorable for their appearance, an order of magnitude estimate of the dislocation density can be determined. The dislocation density estimate determined in this manner was 10^9 lines per square centimeter. Observations of chemically etched surfaces of polycrystalline zirconium in the electron microscope by T. Tomiki and S. Ogawa (52) showed that the dislocations revealed by etch pits have a density of nearly 10^9 lines per square centimeter. We can conclude, therefore, with some confidence that the grown-in dislocation network probably has a dislocation density between 10^8 and 10^9 lines per square centimeter in the annealed commercial pure polycrystalline zirconium used in this investigation.

A quantitative measure of the fraction of tensile

strain due to twinning in similar material has been made for tensile deformation at 77°K (38, 40). These measurements show that a low temperature prestrain in transverse zirconium specimens in the range of less than 1 per cent will nucleate numerous fine twins of the forms $\{10\bar{1}2\}$, $\{11\bar{2}2\}$, and $\{11\bar{2}1\}$. The volume fraction measurements for each type of twin show that the $\{11\bar{2}1\}$ type twin is responsible for nearly all of the deformation at these small prestrains. The number of $\{11\bar{2}2\}$ twins is not significant while the small value of the twinning shear 0.17 for $\{10\bar{1}2\}$ twins limits its contribution to the total tensile strain. These $\{11\bar{2}1\}$ twins, nucleated at the low temperature, would necessarily have to intersect the grown-in dislocations of the Frank network. The resulting dislocation-twin intersection structure will be discussed below.

The number of dislocations which intersect the twin boundary can be calculated using the average grain diameter and the estimated dislocation density of the Frank network. The average grain diameter (Figure 1) as measured by the linear intercept method was determined to be approximately 3×10^{-3} centimeters. The resulting cross sectional area of the average grain is, therefore, 7×10^{-6} square centimeters. Assuming that the twins which nucleate at 77°K traverse the entire grain, this will equal the average twin surface area for one half of the twin. Therefore, for a dislocation density of 10^{8} lines per square centimeter the number of dislocations threading the twin is 700. Similarly, for a density

of 10^9 lines per square centimeter the number is 7,000. From these calculations it is evident that the number of dislocations which intersect the twin boundary surfaces is very large.

In order to determine the effect of a dislocation twin boundary intersection, it will be necessary to consider the various types and orientations of dislocations which may exist in the polycrystalline zirconium Frank network. Both 1/3 $[11\bar{2}0]$ and 1/3 $[11\bar{2}3]$ type dislocations should be considered (30). The 1/3 $[11\bar{2}0]$ type dislocations in the basal plane are associated with three types of slip deformation in the hexagonal crystal structure of zirconium: $\{10\bar{1}0\}$ prism slip, $\{00\bar{0}2\}$ basal slip, and $\{10\bar{1}1\}$ pyramidal slip. Of these three the most important deformation mode is prism slip. The significance of the 1/3 $[11\bar{2}3]$ type dislocation in deformation of zirconium has not been completely resolved. Dislocations of this type were first observed in zinc crystals by R. L. Bell and R. W. Cahn (53) and have also been observed by P. B. Price (54, 55, 56) in cadmium and zinc crystals. In addition, D. H. Baldwin (57) has observed $\{11\bar{2}2\}$ slip in zirconium deformed at low temperatures by torsion. This deformation may be due to dislocations with a 1/3 $[11\bar{2}3]$ Burgers vector.

In the hexagonal crystal there exist three orientations for the 1/3 $[11\bar{2}0]$ type dislocations, a_1, a_2, and a_3, which lie 120 degrees apart in the basal plane. Of these three only one will shear, the $\{11\bar{2}1\}$ twin on intersection in a

direction normal to its projection on the basal plane. Figure 27 shows the relation between the $\{11\bar{2}1\}$ plane and the "a" type slip dislocations. The intersection of the a_1 dislocation with the $\{11\bar{2}1\}$ twin would result in a shear displacement of two $\{11\bar{2}1\}$ planes. Each of the other two dislocations of the 1/3 $[11\bar{2}0]$ types, a_2 and a_3, would intersect the twin with a shear displacement of only one $\{11\bar{2}1\}$ interplanar spacing since they are both arranged at angles of 60 degrees to the projection of the $\{11\bar{2}1\}$ twin plane and the basal plane. The 1/3 $[11\bar{2}3]$ dislocations would shear the twin boundary in an analogous fashion producing shear steps on the twin of either 0, 1, 2, or 3 interplanar spacings.

The shear steps which result from the intersection of these dislocations with the $\{11\bar{2}1\}$ type twins leave corresponding twinning dislocations of either 0, 1, 2, or 3 "t" Burgers vectors along the twin surface (58, 59). It is possible for the higher number of "t" type twinning Burgers vector dislocations on the surface of the twin to dissociate so as to form groups of single "t" dislocations. However, a twinning dislocation of Burgers vector 2t puts the lattice back in registry across the twin plane. A 2t twinning dislocation may, therefore, be a mobile dislocation on the twin surface while a 1t or 3t Burgers vector dislocation may not be mobile. The main point of the above discussion is that not all twin boundary dislocation intersections need lead to the formation of mobile twinning dislocations on the twin

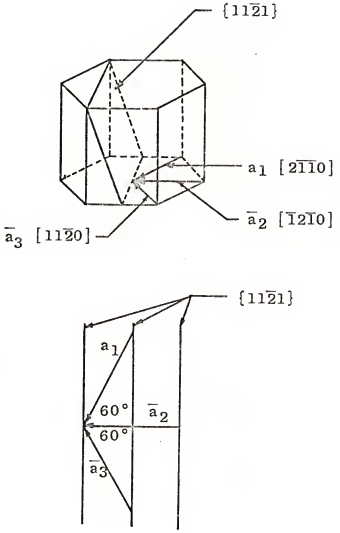

Figure 27. The relationship between the {11$\bar{2}$1} plane and the "a" <11$\bar{2}$0> slip dislocations in the zirconium hexagonal crystal structure.
(a) {11$\bar{2}$1} twin plane in hexagonal crystal.
(b) Projection of {11$\bar{2}$1} twin planes on basal plane showing their intersections with the a_1, a_2, and a_3 slip dislocations.

surface. Those which are mobile probably have a 2t Burgers vector.

Figure 28 shows the relationship between the $\{11\bar{2}1\}$ twin habit plane, the "t" Burgers vector and the unit "a" vector in the basal plane. The magnitude of "t" is given by the following relations:

$$t = 2h \tan 18°$$

where h is the perpendicular distance between $\{11\bar{2}1\}$ planes, and

$$2h = a \cos 18°.$$

Therefore,

$$t = a \cos 18° \tan 18°$$

$$t = a \sin 18°$$

$$t = 3.2 \times 10^{-8} \sin 18° \text{ cm}$$

$$t = 1.0 \times 10^{-8} \text{ cm}.$$

The direction of the "t" Burgers vector lies along the N_1 shear direction, $[\bar{1}1\bar{2}6]$, of the $\{11\bar{2}1\}$ type twin for a dislocation of edge orientation.

Model of Twin Surface

The $\{11\bar{2}1\}$ type twins nucleated at 77°K during the prestrain intersect the grown-in dislocation of the Frank network. At the intersection of each twin and mobile dislocation, a step is created on the boundary corresponding to a dislocation of probable Burgers vector 2t. On subsequent stressing these twinning dislocations can spiral outward between the Frank network increasing the thickness of the twin.

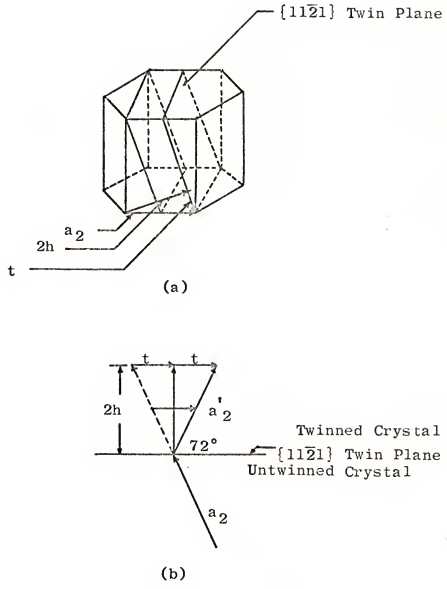

Figure 28. (a) The relation between the {11$\bar{2}$1} twin habit plane, the twinning dislocation (t) Burgers vector, and the unit <11$\bar{2}$0> vector in the basal plane.
(b) View along twin plane between twinned and untwinned crystal showing t Burgers vector dislocation.

This model is analogous to the model of crystal growth proposed by F. C. Frank (60, 61). In order to explain the discrepancy between the theoretical and observed supersaturation concentrations required to grow two-dimensional monolayers of crystals from the vapor, Frank proposed that a dislocation in the screw orientation which emerged normally to the crystal surface would provide a molecular terrace on which growth could continue without the need for fresh two-dimensional nucleation. The model requires a dislocation with a Burgers vector in which the projection normal to the plane of growth is equal to the crystal interplanar spacing. Such a dislocation would provide a "spiral staircase" for indefinite growth at low supersaturation levels.

The growth mechanism for the twin case is similar. A. H. Cottrell and B. A. Bilby (24) first proposed a pole mechanism for the normal growth of a twin in body-centered cubic materials. The pole dislocation mechanism for hexagonal materials was first presented by N. Thompson and D. J. Millard (25). The pole dislocation must have a Burgers vector with a component normal to the twin plane K_1 equal to a multiple of the twin plane separation. As the twinning dislocation moves, it rotates about the pole dislocation; and the twin surface is displaced outward.

The ledges in the mechanism of crystal growth proposed by Frank are analogous to the twinning dislocations in the model for twin growth. The twin boundaries observed in the zirconium microstructure (Figure 6) are relatively straight

and are assumed to be nearly coherent. Therefore, it is reasonable to assume, as Frank did, that poles of opposite type are interconnected. When a single pole is near the grain boundary, its associated twinning dislocation can be assumed to run out to the grain edge forming a single spiral step on the twin surface. Poles of opposite type would form closed terraces of twinning dislocations analogous to the Frank-Read source for dislocation multiplication. Therefore, many poles can intersect the twin and still result in a nearly coherent boundary. Assuming all the dislocations intersecting a twin would have the same sign, 700 or 7,000 dislocations would have a maximum step height of the order of 700 to 7,000 Å. This would be difficult to detect optically.

In order to determine the factors which control twin growth, it is necessary to consider the way in which a ledge or terrace on the twin boundary can move through non-moving poles and their associated dislocations. Figure 29 shows two possible dislocation configurations which can result from the outward movement of a twin terrace through the nearby network of non-moving dislocation poles. In part (a) a terrace moving from left to right intersects a dislocation pole forming a terrace of twice the usual height. The dislocation loops around and pinches together as segments of opposite sign intersect and pass through the non-moving pole. An analogous situation occurs, part (b), when the moving terrace intersects a pole from right to left. In general,

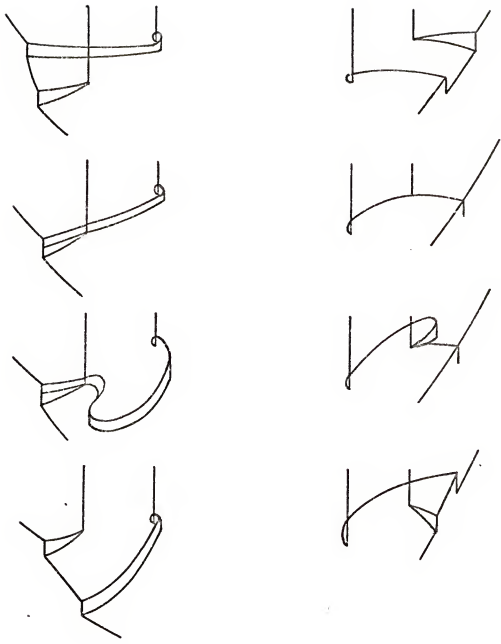

Figure 29. Two possible configurations for the growth of a twin terrace through non-moving dislocation poles.
(a) Twin terrace moving from left to right.
(b) Twin terrace moving from right to left.

therefore, there is apparently no reason why an expanding ledge cannot move across the twin boundary and increase the twin thickness.

The factor which controls the movement of the twinning dislocation ledges is the radius of curvature into which the expanding ledge must be bent in passing through the non-moving dislocation poles. The situation is completely analogous to the Frank-Read mechanism for dislocation multiplication and growth. The model for twin growth can be thought of as a single Frank-Read source at the center of the twin boundary. As shown above, the average dislocation density of the Frank network is approximately 10^8 lines per centimeter squared. This implies that the mean separation of dislocations is about 10^{-4} centimeters.

$$d = \sqrt{\frac{1}{\rho}}$$

$$d = \sqrt{\frac{1}{10^8}} = 10^{-4} \text{ cm}$$

The radius of a corresponding Frank-Read source would, therefore, be approximately 5×10^{-5} centimeters.

$$r = \frac{d}{2} = \frac{10^{-4}}{2} = 5 \times 10^{-5} \text{ cm}$$

According to Cottrell (17) the shear stress σ, dislocation line T, radius of curvature r, and Burgers vector b, are related in the following manner for a curved dislocation loop:

$$\sigma = \frac{T}{br}$$

The line tension of a circular dislocation as a function of its radius has been evaluated by D. J. Bacon and A. G. Crocker (62). Figure 30 shows this line tension function. The line tension is plotted in terms of the shear modulus μ, and the Burgers vector squared b^2, as a function of the radius r of the dislocation loop. For a loop radius of 5×10^{-5} centimeters, the corresponding line tension is $0.72\ \mu b^2$. The Burgers vector length of a mobile twinning dislocation was shown above to be probably 2.0×10^{-8} centimeters. Using a shear modulus of 5×10^{6} psi (63, 64) for polycrystalline zirconium, the shear stress necessary to bend an initially straight twinning dislocation to its critical curvature is approximately 1,440 psi.

$$\sigma = \frac{0.72 \times 5 \times 10^{6} \times 2.0 \times 10^{-8}}{5 \times 10^{-5}} = 1{,}440 \text{ psi}$$

Using a length of 1.0×10^{-8} centimeters corresponding to a twinning dislocation of length t, the calculated shear stress would be 720 psi.

The nearly symmetrical shape of the approximate equilibrium stress-strain curves shown in Figures 21 through 26 indicates that both on loading and unloading the twinning dislocations are bent from an initially curved position through the position of zero stress to the critical curvature of opposite sign. The residual bowing of the dislocations in the direction opposite to the initial loading stress results

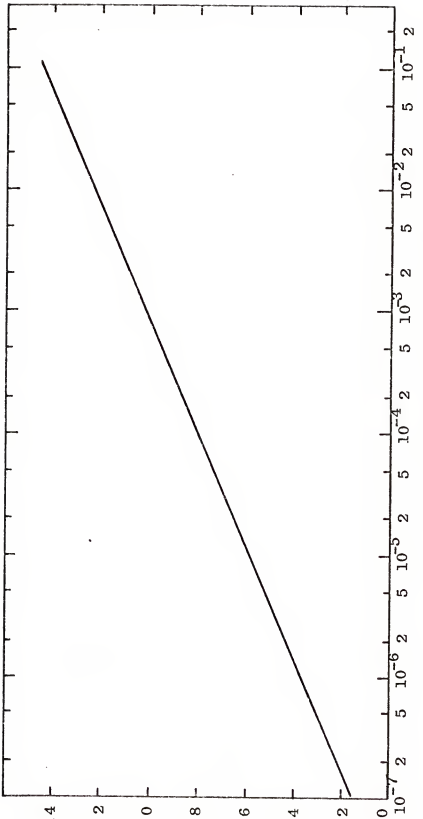

Figure 30. The line tension of a circular dislocation as a function of its radius of curvature.

from a back stress due to dislocations which moved over the twin surfaces in front of the sources during the prestrain treatment at 77°K. Thus, the shear stress required to cause large scale nonelastic strain development or recovery would be twice that calculated above for both the loading and unloading portion of the stress-strain diagram. Using this assumption together with a value of the orientation factor for $\{11\bar{2}1\}$ twins of 0.42 (40), the critical tensile stress for anelastic strain development would be 6,880 and 3,440 psi respectively for Burgers vectors of lengths 2t and 1t. Table 2 shows the experimental values of the tensile stresses for anelastic strain development for the specimens shown in Figures 19 through 26. The average value for these seven specimens was 4,800 psi. The agreement between this average stress and those calculated from the above relations is very good considering the hypothetical nature of the proposed model. The correlation indicates, therefore, that the basic assumptions of the model may be correct.

Model for Back Stress Limiting Twin Growth

The actual twins as nucleated in the prestrained zirconium are nearly always straight-sided. This implies that the boundaries are under a condition of zero stress and are essentially coherent. As can be seen by the microstructure of the prestrained zirconium, Figures 6 through 8, most of the twins end at a grain boundary. The shear associated with an average twin is of the order of 100 Å (40). A shear of this

magnitude associated with the twins must produce a very large stress in the grains facing the ends of the twins. It is logical to assume that the stress concentration ahead of the twins is partially relaxed by slip in these grains. A model of the twinned region which conforms to the above assumptions is shown in Figure 31(a). Considering these assumptions, it is not unreasonable to simplify this model further. An equivalent model is shown in Figure 31(b). It is reasonable to assume that the dislocation distribution at the twin edges and adjoining grains can be replaced by a single dislocation at the twin boundary. The single dislocation would have a Burgers vector equivalent to the total Burgers vector of the twinning dislocations plus the slip dislocations in the adjoining grains. The center of the dislocation distribution must, therefore, lie close to the edge of the twin.

The effective Burgers vector of the dislocation distribution as depicted at the edge of the twin can be determined in the following way. The external strain which results from a dislocation moving on its slip plane is given by Cottrell (17) as

$$\gamma = \frac{A}{V} b$$

where A is the area through which the dislocation moves, V is the specimen volume, and b the dislocation Burgers vector. This may be generalized for the conditions under consideration to

(a) (b)

Figure 31. Schematic illustration of $\{11\bar{2}1\}$ twin interface showing (a) the probable dislocation distribution along the twin and in the adjoining grains and (b) the proposed model substituting a single dislocation at the twin edge.

$$\epsilon_n = \frac{S_v}{2} \bar{m} b_{eff}$$

where ϵ_n is the total relaxable tensile strain due to the motion of the $\{11\bar{2}1\}$ twin boundaries, S_v is the surface area per unit volume of the twins, $\bar{m}$ the average orientation factor to account for the fact that the measured strain is tensile while the twinning displacements are shear strains, and b_{eff} is the effective Burgers vector at the twin edge. Figure 32 shows the measured surface area of $\{11\bar{2}1\}$ twins as a function of prestrain for prestrains of less than 1 per cent by rolling and tensile deformation (38). From this figure it is seen that the surface area per unit volume for this type of twin is nearly linearly related to the magnitude of prestrain. Figure 33 shows the experimentally determined values of the total relaxable strain as a function of prestrain as measured in the various tests used in this investigation. Here again, for prestrains of less than 1 per cent the relaxable strain can be nearly linearly related to the prestrain. Therefore, substituting these results into the above equation, the effective Burgers vector is given by the relation

$$b_{eff} = \frac{2K''}{\bar{m}K'}$$

where $S_v = K'\epsilon_p$ and $\epsilon_r = K''\epsilon_p$. Using the values of $K' = 2.25 \times 10^5$ cm^{-1} and $K'' = 6.25 \times 10^{-2}$ as determined from Figures 32 and 33, the calculated value of the effective Burgers vector is 130×10^{-8} centimeters.

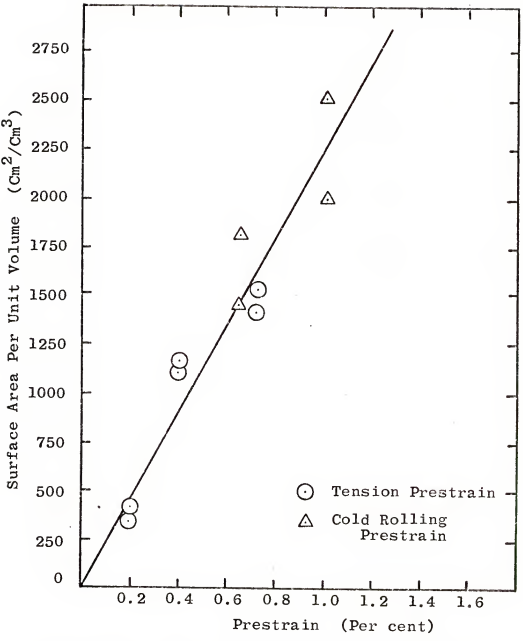

Figure 32. Measured surface area of $\{11\bar{2}1\}$ twins as a function of the amount of prestrain.

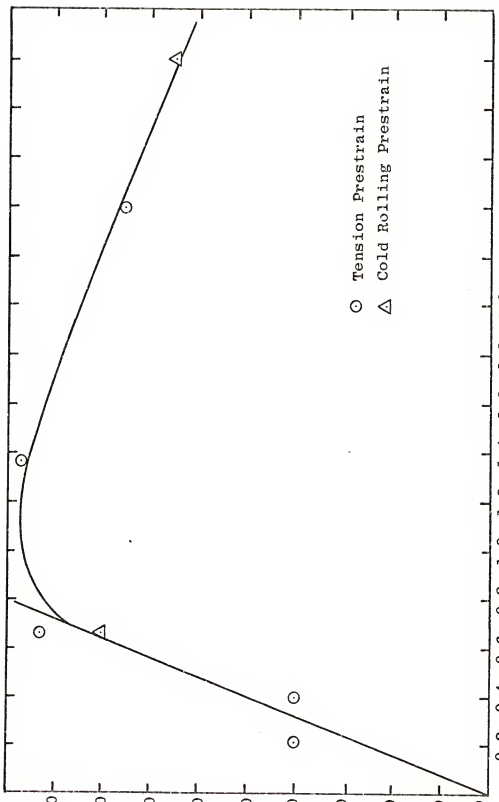

Figure 33. Total relaxable or anelastic strain at 15,000 psi as a function of prestrain for zirconium specimens tested at 80°C.

Under near equilibrium conditions in which almost all of the relaxable strain has been generated, the applied stress at the source of the twinning dislocation would be reduced to σ_c, the critical stress for dislocation motion. The back stress at the source for a dislocation loop with an effective Burgers vector of 130 x 10^{-8} centimeters can be calculated using the formula introduced above.

$$\sigma = \frac{T}{br}$$

In this instance r is the average grain radius (1.5 x 10^{-3} centimeters) and b is the effective Burgers vector (130 x 10^{-8} centimeters). From Figure 30, the line tension T of a dislocation loop is given as 1.04 μb^2. The back stress is then

$$\sigma = \frac{1.04 \times 5 \times 10^6 \times 130 \times 10^{-8}}{1.5 \times 10^{-3}} = 4{,}500 \text{ psi}$$

The observed average applied stress which this back stress would necessarily balance under near equilibrium conditions for the seven experimental tests run at 80°C for various prestrain amounts was 4,360 psi (Table 2).

$$\sigma = (\sigma_m - \sigma_c)\ \bar{m}$$

$$\sigma = (15{,}200 - 4{,}800)\ 0.42 = 4{,}360 \text{ psi}$$

The excellent agreement between the calculated value and the observed value tends to show that the assumptions made in developing this twin model are valid.

Shape of the Two Cycle Hysteresis Loop

The shape of the two cycle hysteresis loop can be explained using the model of twin growth presented above in combination with the observation that the movement of twinning dislocations along the twin matrix interface was thermally assisted. On application of the load the twinning dislocations remained immobile until the critical stress was reached for operating the Frank-Read sources. Up to that point the material responded in an elastic manner following the unrelaxed modulus. When the critical stress for operating the smallest Frank-Reed source was reached, the twinning dislocations assisted by thermal energy were able to move out on the twin matrix interface to the grain boundaries. Here they were held up and exerted a back stress at the source to reduce the applied stress. When the load was applied sufficiently slowly, the dislocations were able to move in a manner which maintained the back stress in equilibrium with the applied stress in excess of the critical stress for operating the Frank-Read source. In this instance the specimen followed the relaxed modulus at each point of the stress-strain curve above σ_c. On unloading the twinning dislocations remained relatively stationary until the critical stress for operating the Frank-Read source was reached in the opposite direction. Here, the back stress due to the dislocation pile-up along the grain edges aided in causing the twinning dislocations to reverse their motion. Again,

when the load was removed slowly, the dislocations were able to maintain a back stress in equilibrium with the applied stress and the stress-strain curve followed the relaxed modulus line. The closed loop configuration for the stress cycle as shown in Figure 19 was the result.

When the load was applied or removed at faster rates so that the dislocations could not maintain an equilibrium back stress on the Frank-Read source, a different stress-strain configuration resulted. On loading, the stress at which significant deviation from the unrelaxed modulus occurred was higher depending on the rate of loading. Likewise, the slope of the stress-strain curve at higher stresses was at an intermediate value between the unrelaxed and the relaxed moduli and varied with the applied stress. At any particular spot on the loading curve the dislocations at the twin edges were less than fully developed. An additional component of anelastic strain ϵ^* formed with time when the loading was stopped. A similar situation developed on unloading. When zero stress was reached, a component of anelastic strain remained in the test piece and decayed with time to zero. This resulted in the anelastic aftereffect. Figure 34 shows the tensile stress-strain curve for a transverse zirconium specimen strained 0.65 per cent by tension at 77°K. The test was run at 80°C at a strain rate of 2.7×10^{-5} seconds^{-1}. Superimposed on this curve is the nearly equilibrium stress-strain curve for this specimen. This figure shows the extent of anelastic strain which can be expected to

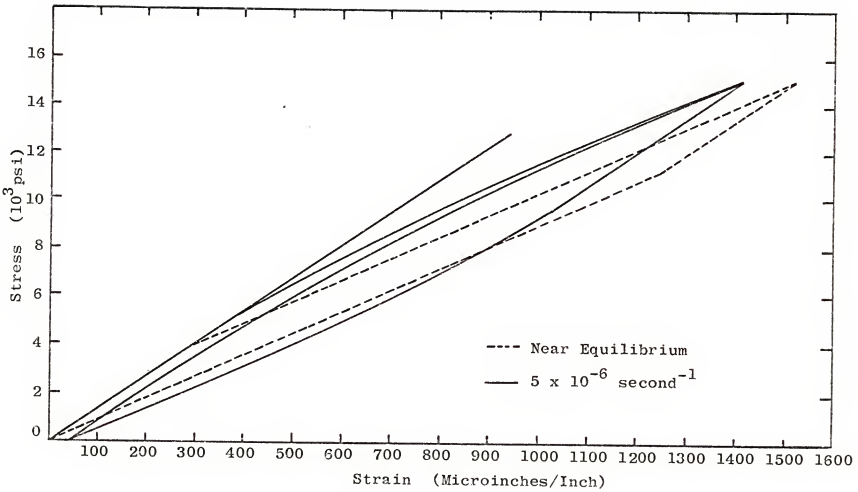

Figure 34. Comparison between the tensile near equilibrium and the 5 x 10^{-6} second^{-1} strain rate stress-strain curves at 80°C for cyclically loaded zirconium specimen prestrained 0.65 per cent by tension at 77°K.

develop at each point on the stress-strain curve. This relaxable strain is the difference between the two curves at any constant stress level. On loading and unloading significant anelastic strain development did not occur until the corresponding position on the equilibrium diagram was passed.

Elastic Aftereffect

The equations governing the elastic aftereffect phenomena have been presented in detail by R. E. Reed-Hill and E. P. Dahlberg (26, 27). The relationships for the relaxation of strain at constant stress and the relaxation of stress at constant strain were derived from the basic equation of strain relaxation due to Kuhlman (28). The relaxation was assumed to result from a reversible thermally activated process which occurred at a number of relaxation centers embedded in an elastic matrix.

$$\dot{\epsilon} = \gamma N \nu e^{\frac{-(\Delta F^{\ddagger} - V\sigma_s)}{RT}} - \gamma N \nu e^{\frac{-(\Delta F^{\ddagger} + V\sigma_s)}{RT}} \qquad [1]$$

In this equation $\dot{\epsilon}$ is the strain rate, $\Delta F^{\ddagger}$ the free energy of activation for the mechanism controlling the strain relaxation, V an activation volume, R the gas constant, T the absolute temperature, ν the Debye frequency, γ the strain contribution of a unit process, and N the number of relaxation centers per unit volume. σ_s is the effective or average resolved stress at the relaxation center corresponding, in this instance, to the instantaneous stress on the twinning dislocations minus the critical stress for

operation of the Frank-Read source. This equation may be written

$$\dot{\epsilon} = 2Ae^{-\frac{Q}{RT}} \sinh \frac{V\sigma_s}{RT} \qquad [2]$$

where $A = \gamma N \nu e^{\frac{\Delta S^{\pm}}{R}}$ and $\Delta S^{\pm}$ and Q are the activation entropy and activation energy of the relaxation mechanism.

At this point it is necessary to introduce the concept of the relaxable strain in order to relate σ_s to ϵ and integrate equation [2]. To do this the following equation is introduced.

$$M_r \epsilon = \sigma_a - \sigma_c \frac{(M_u - M_r)}{M_u} - \frac{(M_u - M_r)}{\bar{m} M_u} \sigma_s \qquad [3]$$

M_r and M_u are the relaxed and unrelaxed moduli respectively, σ_a the applied constant tensile stress, σ_c the tensile stress corresponding to the point where the Frank-Read sources of the twinning dislocations first begin to operate, and $\bar{m}$ an average orientation factor that accounts for the fact that the effective stress at the relaxation center σ_s is a shear stress and not a tensile stress. This equation is of the form first derived by Zener (29) for the case of strain relaxation at slip bands. In this instance it has been modified to account for the stress necessary to initiate the twinning dislocation loop motion. Solving this equation for σ_s yields

$$\sigma_s = \frac{\bar{m} M_u M_r}{(M_u - M_r)} (\epsilon_r - \epsilon) \qquad [4]$$

Where ϵ_r the total relaxed or maximum strain is given by

$$\epsilon_r = \frac{1}{M_r} \left[\sigma_a - \frac{(M_u - M_r)}{M_u} \sigma_c \right] \qquad [5]$$

The strain capable of relaxing at any given instant is $(\epsilon_r - \epsilon)$, the relaxable strain, and this strain will be denoted as ϵ^*.

On substituting this equation into equation [4] and noting that $\dot{\epsilon}^* = -\dot{\epsilon}$, the following relation is derived.

$$\dot{\epsilon}^* = -2Ae^{-\frac{Q}{RT}} \sinh \frac{\alpha \epsilon^*}{RT} \qquad [6]$$

where

$$\alpha = \frac{\bar{m} M_u M_r V}{(M_u - M_r)} \qquad [7]$$

Integration of equation [6] yields

$$\ln \tanh \frac{\alpha \epsilon^*}{2RT} = -\frac{t}{\tau_\sigma} + C \qquad [8]$$

where C is a constant of integration and

$$\frac{1}{\tau_\sigma} = \frac{\bar{m}\ 2\ M_u\ M_r\ V\ Ae^{-\frac{Q}{RT}}}{(M_u - M_r)\ RT} = \frac{2\alpha A}{RT}\ e^{-\frac{Q}{RT}} \qquad [9]$$

For the case of the elastic aftereffect at zero stress, equation [8] becomes

$$\ln \tanh \frac{\alpha\epsilon}{2RT} = \tanh \frac{\alpha\epsilon_o}{2RT} = -\frac{t}{\tau_\sigma} \qquad [10]$$

or

$$\tanh \frac{\alpha\epsilon}{2RT} = \tanh \frac{\alpha\epsilon_o}{2RT}\ e^{-\frac{t}{\tau_\sigma}} \qquad [11]$$

By a suitable transformation of this equation, a more convenient expression can be derived which relates the relaxable strain ($\epsilon^* = \epsilon$ for the elastic aftereffect) explicitly to the time t. This expression is

$$\epsilon^* = -\frac{RT}{\alpha} \ln \tanh \frac{t + t_o}{2\tau_\sigma} \qquad [12]$$

Experimental Verification of Elastic Aftereffect Equations

The elastic aftereffect data shown in Figures 15 and 16 for zirconium specimens prestrained 0.65 per cent by tension and 3.0 per cent by cold rolling respectively can be accurately described by the above derived equations. The solid curves in these figures are drawn to conform to equation [12] using values of α equal to 45×10^6 and 25×10^6

calories per mole. It is evident from the figures that the close correspondence between the theoretical curves and the experimental curves verifies the use of the elastic after-effect formulations for the detwinning of $\{11\bar{2}1\}$ twins as described in the above model.

Since the value of α is simply related to the anelastic strain through equation [12], it must be evaluated independently. Using equation [10], the above values of α were determined as those which most nearly made a plot of $\ln \tanh \frac{\alpha\epsilon}{2RT}$ a linear function of time. Such a plot is shown for the data of Figure 15 in Figure 35. Values of α above and below 45×10^6 do not yield straight lines in this figure. Values of α of 45×10^6 and 25×10^6 calories per mole for these two specimens also yielded good straight lines for the aftereffect data obtained at the other temperatures. Plots of $\ln \tanh \frac{\alpha\epsilon}{2RT}$ versus time curves at various temperatures for the above two specimens are shown in Figures 36 and 37.

From equation [10] it is seen that from the slopes of the $\ln \tanh \frac{\alpha\epsilon}{2RT}$ versus time curves the relaxation time at constant stress τ_σ can be calculated. From equation [9] it follows that

$$\ln \frac{\tau_\sigma}{T} = \frac{Q}{RT} + \ln \frac{R}{2\alpha A} \qquad [13]$$

so that a plot of $\ln \frac{\tau_\sigma}{T}$ as a function of the reciprocal of the absolute temperature which is linear should give an

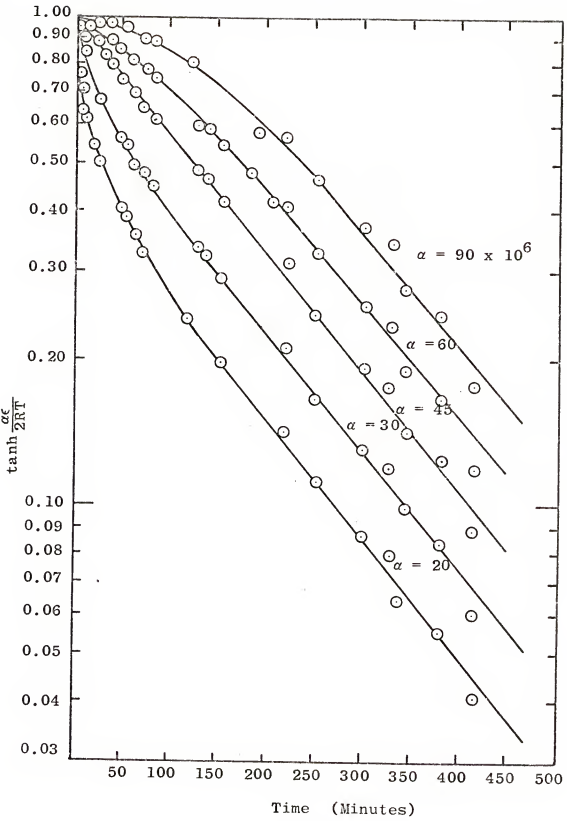

Figure 35. Curves of ln tanh $\alpha\epsilon/2RT$ as a function of time for various values of α corresponding to the data obtained in Figure 15 at 40°C.

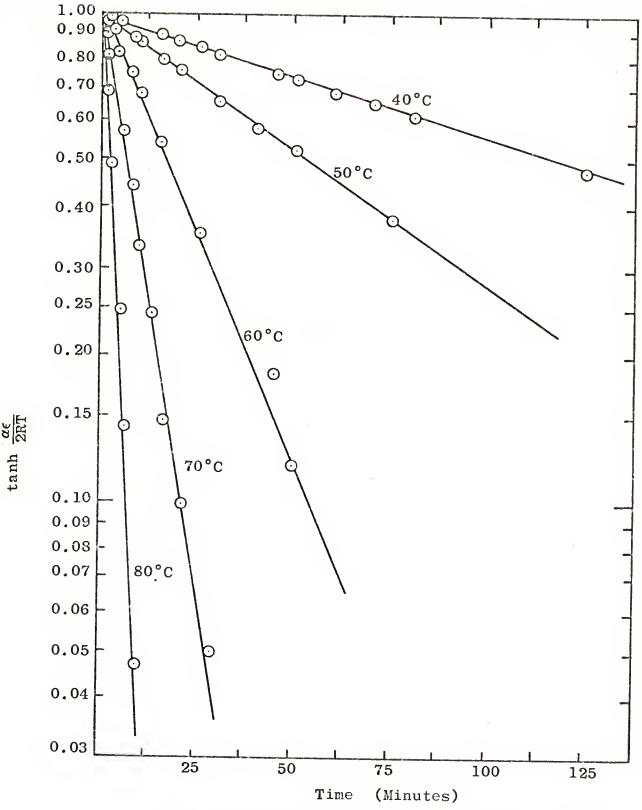

Figure 36. Curves of ln tanh $\alpha\epsilon/2RT$ versus time for the elastic aftereffect at various temperatures of a zirconium specimen prestrained 0.65 per cent by tension. (Corresponding to Figure 15)

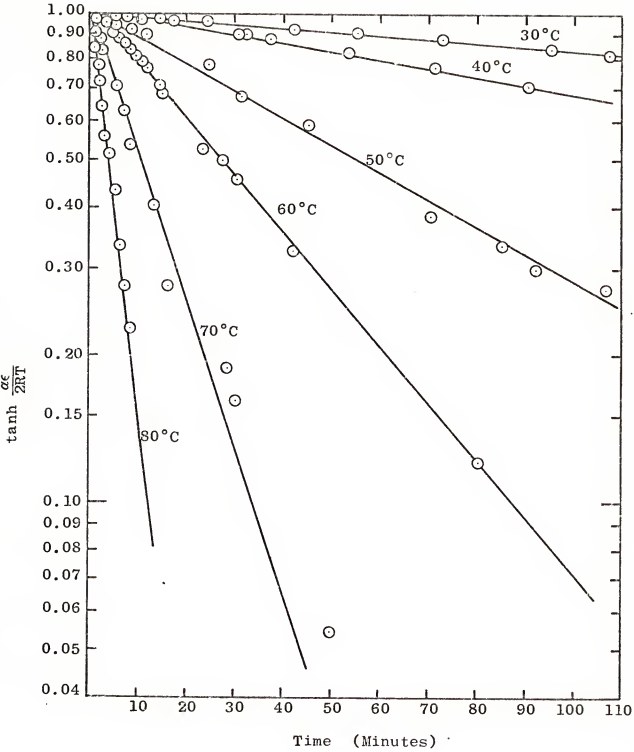

Figure 37. Curves of ln tanh $\alpha\epsilon/2RT$ versus time for the elastic aftereffect at various temperatures of a zirconium specimen prestrained 3.0 per cent by cold rolling. (Corresponding to Figure 16)

indication of the activation energy for the mechanism controlling the strain recovery process. Such a plot is shown in Figure 38 for the two sets of data shown in Figures 36 and 37 and for an additional specimen prestrained 1.36 per cent by tension. The data plotted in this manner give very good straight lines over the temperature interval of experimentation. The slopes give an average activation energy of 23,000 calories per mole for the mechanism controlling twin boundary movement.

The activation volume for the mechanism controlling the movement of twin boundaries can be determined by the use of equation [7]. By using values of α determined as described above together with values of the relaxed modulus and the unrelaxed modulus determined experimentally (Figures 19 through 26) a reasonably accurate value of the activation volume can be calculated. The value of $\bar{m}$ of 0.42 has been determined previously. Table 3 lists seven specimens for which appropriate data have been measured to determine the activation volume. This table shows the values of α, M_u, M_r, and V for these seven tests run at 80°C. The calculated values of V/b^3 are fairly constant for each of the specimens. The average value of the activation volume for the seven specimens is 67 b^3.

Mechanism Controlling Twin Boundary Movement

The model for twin growth described above would suggest that the controlling mechanism for twin boundary movement is

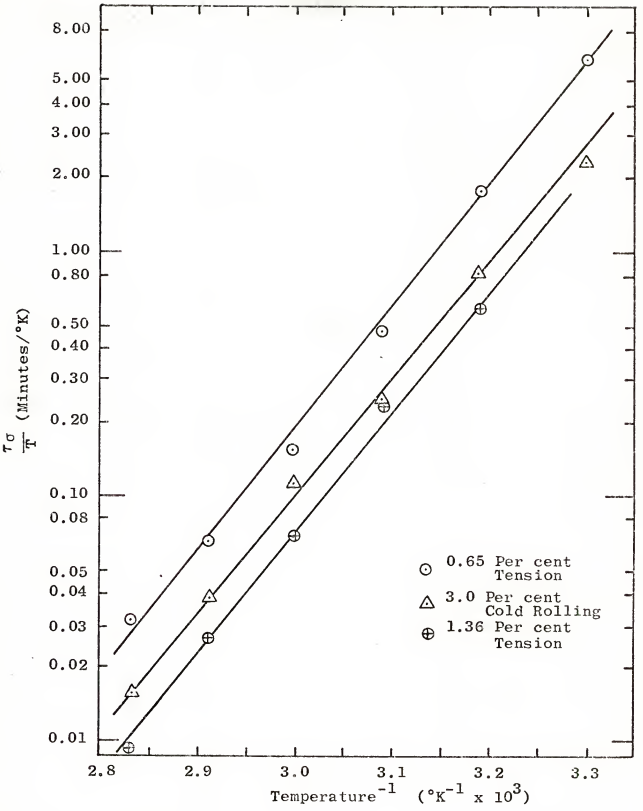

Figure 38. Activation energy plot for the data of Figures 36 and 37.

TABLE 3

ACTIVATION VOLUME MEASUREMENTS

Prestrain (per cent)	Unrelaxed Modulus (10^6 psi)	Relaxed Modulus (10^6 psi)	α (10^6 cal. per mole)	V (10^{-21} cm^3)	V/b^3
0.2 T	13.0	10.6	38	1.67	51
0.4 T	12.3	9.9	30	1.50	46
0.64 T	13.4	8.8	23	2.24	68
1.36 T	12.5	8.0	20	2.28	70
2.4 T	13.1	8.8	20	1.89	58
0.65 CR	13.5	9.1	45	4.05	124
3.0 CR	12.8	9.5	25	1.89	52

T = Tension Prestrain

CR = Cold Rolling Prestrain

a slip process. The shear displacement associated with a change in twin thickness may result in large stress concentrations near the twin edges. According to J. Fridel (65) the stresses ahead of the twin are given by the formula

$$\sigma_1 = \frac{2L}{\mu b} \sigma_a^2$$

where σ_a is the applied shear stress on the twin and L is the twin diameter. For the case considered here, the stress at the twin edge would exceed the yield stress of the zirconium by nearly an order of magnitude. Some relaxation of this high stress would be expected. As slip proceeded in the adjoining grains, additional twin growth would be possible. A similar situation would be expected to exist on collapse of the twin on unloading.

The activation volume, approximately 67 b^3, and the corresponding activation energy, 23,000 calories per mole, are both in agreement with this proposed slip mechanism controlling twin boundary movement. The activation energy value agrees with those values cited in the limited amount of data available in the literature concerned with slip deformation in zirconium near room temperature (66, 67). In addition, tests by J. S. Wolf (68) on transverse and longitudinal zirconium specimens showed an activation energy determined from creep tests which was very nearly identical to that determined in this investigation. Figure 39 shows a plot of the logarithm of the cyclic period of stress adjustment

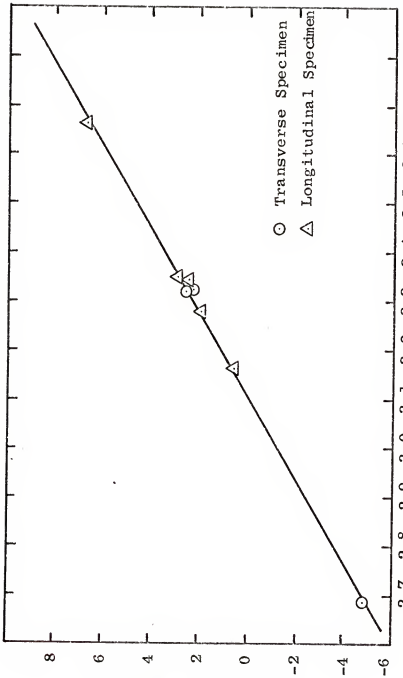

Figure 39. The tensile machine relaxation period for room temperature creep as a function of the reciprocal of the absolute temperature for longitudinal zirconium specimens.

on the automatic load maintainer of the Instron tensile machine as a function of the reciprocal temperature for several creep tests of pure zirconium. The experimental techniques used in these creep tests have been described previously (41). The activation energy of 23,800 calories per mole determined from this set of data is in excellent agreement with that measured for twin boundary movement. The value of 67 b^3 for the activation volume is consistent with a Peierls mechanism of slip deformation for hexagonal close-packed materials. The meaning of the activation volume together with various values corresponding to different supposed mechanisms has been outlined recently by J. E. Dorn and S. Rajnak (69). In view of these observations it seems reasonable to conclude that the mechanism controlling the movement of the $\{11\bar{2}1\}$ twin boundaries in the transverse zirconium specimens is a slip mechanism taking place in the grains adjacent to the twin edges.

CHAPTER V

CONCLUSIONS

1. Nucleation of numerous $\{11\bar{2}1\}$ type twins by prestraining transverse specimens of zirconium at 77°K imparts a large room temperature mechanical hysteresis and elastic after-effect to the material.

2. The mechanical hysteresis is a sensitive function of the amount of prestrain reaching a maximum for specimens pre-strained approximately 1 per cent.

3. The hysteresis losses increase with increasing maximum cyclic load, decrease with a decrease in temperature between -72 and 80°C, and decrease with increases in the applied strain rate.

4. The elastic aftereffect obeys an equation for strain at constant stress of the form

$$\epsilon^* = -\frac{RT}{\alpha} \ln \tanh \frac{t + t_o}{2\tau_\sigma}$$

5. A model of twin growth analogous to the Frank mechanism of crystal growth is proposed to account for the anelastic effects.

6. Experimental verification of the model is found in the nucleation stress for Frank-Read sources of twinning dislocations and in the back stress at the dislocation sources due to pile-ups of dislocations at the grains adjacent to the twin boundary edges.

7. The activation energy and activation volume for the mechanism controlling twin growth were determined to be 23,000 calories per mole and 67 b^3 respectively. These agree very well with a slip process.

BIBLIOGRAPHY

1. Zener, C. M., Elasticity and Anelasticity of Metals, University of Chicago Press, Chicago (1948).

2. Ewing, A., "On Measurements of Small Strains in the Testing of Materials and Structures," Proc. Roy. Soc. London, 58 (1895) 23.

3. Muir, J., "On the Recovery of Iron from Overstrain," Phil. Trans. Roy. Society, 193 (1900) 1.

4. Weber, W., "Uber die Elastizitat der Scidendoden," Paggendorff's Ann., 35 (1834) 247.

5. Haigh, B. P., "Hysteresis in Relation to Cohesion and Fatigue," Trans. Faraday Soc., 24 (1926) 125.

6. Koster, W. and Rosenthat, K., "Die Anderung von Elastizitatsmopul und Dampfung bei der Verformung und Rekrestallistallisation von Messing," F fur Metallkunde, 30 (1938) 345.

7. Richter, V. G., "Uber die Mechenische un die Magnetische Nachwerking des Carbonyleisens," Annalen der Physik, 5 (1938) 683.

8. Snock, J., "Tetragonal Martensite and Elastic Aftereffect in Iron," Physica, 9 (1942) 862.

9. Roberts, J. M. and Brown, N., "Microstrain in Zinc Single Crystals," Trans. AIME, 218 (1960) 454.

10. Bonfield, W. and Li, C. H., "The Friction Stress and Micro-Yielding of Beryllium," ACTA Met. 13 (1965) 317.

11. Roberts, J. M. and Hartman, D. E., "The Temperature Dependence of the Microyield Points in Prestrained Magnesium Single Crystals," Trans. AIME, 230 (1964) 1125.

12. Brown, N. and Lukens, K. F., "Microstrain in Polycrystalline Metals," ACTA Met., 9 (1961) 106.

13. Brown, N. and Ekvall, R.A., "Temperature Dependence of the Yield Points in Iron," ACTA Met., 10 (1962) 1101.

14. Lukas, P. and Klesnil, M., "Hysteresis Loops in Micro-strain Region," Physica Stat. Solidi, 11 (1965) 127.

15. Granato, A. and Lucke, K., "Theory of Applied Damping Due to Dislocations," J. Appl. Phys., 27 (1956) 583.

16. Lucke, K. and Granato, A., "Internal Friction Phenomena Due to Dislocations," Mechanical Properties of Crystals, Wiley and Sons (1957).

17. Cottrell, A.H., Dislocations and Plastic Flow in Crystals, Clarendon Press, Oxford, (1953)

18. Haigh, B.P., "Discussion to Paper by Chalmers," Proc. Phys. Soc. of London, 47 (1935) 745.

19. Chalmers, B., "The Twinning of Single Crystals of Tin," Proc. Phys. Soc. of London, 47 (1935) 733.

20. Worrell, F.T., "The Structure of Manganese Rich Alloys of Copper and Manganese," Phys. Rev., 72 (1947) 533.

21. Worrell, F.T. and Siefert, A.V., "The Role of Tetragonal Twins in the Internal Friction of Copper Manganese Alloys," J. Appl. Phys., 22 (1951) 1257.

22. Jones, E.R.W. and Munro, W., "The Elastic Hysteresis of Uranium," J. Mech Phys. of Solids, 6 (1953) 182.

23. Birnbaum, H.K. and Read, T.A., "Stress Induced Twin Boundary Motion in AuCd β' and β" Alloys," Trans. AIME, 218 (1960) 662.

24. Cottrell, A.H. and Bilby, B.A., "A Mechanism for the Growth of Deformation Twins in Crystals," Phil. Mag., 42 (1951) 573.

25. Thompson, N. and Millard, D.J., "Twin Formation in Cadmium," Phil. Mag., 43 (1952) 422.

26. Reed-Hill, R.E. and Dahlberg, E.P., "Concerning the Relaxation of Strain at Constant Stress and the Relaxation of Stress at Constant Strain," Trans. AIME, 236 (1966) 679.

27. Reed-Hill, R. E. and Dahlberg, E. P., "Some Effects of Prestrain at 77°K on the Mechanical Properties of Zirconium at Room Temperature," Electrochemical Tech., 4 (1966) 303.

28. Kuhlmann, D., "Zur Theorie der Nachwirkungserscheinangen," Z. Phys., 124 (1947) 468.

29. Zener, C., "Dynamics of Slip Bands," Cold Working of Metals, ASM, Cleveland (1949) 180.

30. Rapperport, E. J. and Hartley, C S., "Deformation Modes of Zirconium at 77°K, 575°K, and 1075°K," Trans. AIME, 218 (1960) 869.

31. Martin J. L. and Reed-Hill, R. E., "A Study of Basal Slip Kink Bands in Polycrystalline Zirconium," Trans AIME 230 (1964) 780.

32. Baldwin, D. H. and Reed-Hill, R. E., "Some Observations of the Deformation Modes of Polycrystalline Hafnium and Zirconium," Trans. AIME, 233 (1965) 248.

33. Rapperport, E. J., "Room Temperature Deformation Processes in Zirconium," ACTA Met., 7 (1959) 254.

34. Rapperport, E. J., "Deformation Processes in Zirconium," ACTA Met., 3 (1955) 208.

35. Sokurskii, Iu. N. and Protsenko, L. N., "Deformation Systems of α-Zirconium," Soviet J. of Atomic Energy, 4 (1958) 579.

36. Reed-Hill, R. E., Slippy, W. A., Jr., and Buteau, L. J., Jr., "Determination of Alpha Zirconium $\{11\bar{2}1\}$ Twinning Elements Using Grain Boundary Rotations," Trans. AIME 227 (1963) 976.

37. Reed-Hill, R. E., "Third Quarterly Progress Report," AEC Contract No. AT(38-1)-252 (1962).

38. Reed-Hill, R. E. and Caldwell, F. W., "Eleventh Quarterly Progress Report," AEC Contract No. AT(38-1)-252 (1964).

39. Reed-Hill, R. E., "Role of Deformation Twinning in the Plastic Deformation of Polycrystalline Anisotropic Metal," Deformation Twinning, Gordon and Breach (1963) 295.

40. Reed-Hill, R.E., Buchanan, E.R., and Caldwell, F.W., "A Quantitative Measurement of the Fraction of Tensile Strain Due to Twinning in Polycrystalline Zirconium at 77°K," Trans. AIME, 233 (1965) 1716.

41. Reed-Hill, R.E., "First Quarterly Progress Report," AEC Contract No. AT (38-1)-252, (1961).

42. Reed-Hill, R.E. and Caldwell, F.W., "An Analysis of the Texture of a Zirconium Specimen Based on Measurements of the Surface Distribution of Basal Plane Traces," Part II, Fifth Quarterly Progress Report, AEC Contract No. AT(38-1)-252 (1963).

43. Rittenhouse, P.L. and Picklesimer, M.L., "Metallurgy of Zircoloy-2,Part I. The Effect of Fabrication Variables on the Anisotropy of Mechanical Properties," ORNL-2944, UC-25-Metallurgy and Ceramics (1960).

44. Slippy, W.A., Jr. and Lee, C.C., "Metallographic Techniques for Zirconium and Zircoloy-2," Part IV, Fifth Quarterly Progress Report, AEC Contract No. AT(38-1)-252 (1963).

45. Carnahan, R.D. and White, J.E., "Some Comments on Strain Gage Techniques for Determining Microstrain," Trans. AIME, 230 (1964) 249.

46. Frank, F.C., "Report of Pittsburgh Conference of Plastic Deformation of Crystals," (Washington-Carnegie Institute of Technology, Office of Naval Research) (1950) 100.

47. Bailey, J.E., "The Effect of Impurity on the Dislocation Arrangement in Deformed Polycrystalline Zirconium," Proc. 5th Int. Congress for Electron Microscopy, Academic Press, New York (1962).

48. Bailey, J.E., "Electron Microscope Studies of Dislocations in Deformed Zirconium," J. of Nuclear Matls., 1 (1962) 300.

49. Keh, A.S., "Work Hardening and Deformation Sub-structure in Iron Single Crystals Deformed in Tension at 298°K," Phil. Mag., 12 (1965) 9.

50. Hirsch, P. B. and Lally, J.S., "The Deformation of Magnesium Single Crystals," Phil. Mag., 12 (1965) 595.

51. Bailey, J.E., "Electron Microscope Observations on the Precipitation of Zirconium Hydride in Zirconium," ACTA Met., 11 (1963) 267.

52. Tomiki, T. and Ogawan, S., "Electron Microscope Observation on Chemically Etched Surfaces of Polycrystalline Zirconium," Japan Inst. of Metals J., 24 (1960) 522.

53. Bell, R.L. and Cahn, R.W., "The Dynamics of Twinning and the Interrelation of Slip and Twinning in Zinc Crystals," Proc. Roy. Soc. of London, 239A (1957) 494.

54. Price, P.B., "On Microcreep in Zinc Whiskers," Phil. Mag., 5 (1960) 417.

55. Price, P.B., "Pyramidal Glide and the Formation and Climb of Dislocation Loops in Nearly Perfect Zinc Crystals," Phil. Mag., 5 (1960) 873.

56. Price, P.B., "Nonbasal Glide in Dislocation-Free Cadmium Crystals, I. The (10$\bar{1}$1) 1210 System," J. of App. Phys., 32 (1961) 1746.

57. Baldwin, D.H., "An Investigation of the Effect of Oxygen on the Tensile Deformation of Zirconium," Ph. D. Thesis, University of Florida, Gainesville, Florida (1966).

58. Reed-Hill, R.E., "Ninth Quarterly Progress Report," AEC Contract No. AT(38-1)-252 (1963).

59. Sleeswyk, A.W., "Emissary Dislocations: Theory and Experiments on the Propagation of Deformation Twins in α-Iron," ACTA Met., 10 (1962) 705.

60. Frank, F.C., "The Influence of Dislocations on Crystal Growth," Disc. Faraday Soc., 5 (1949) 48.

61. Frank, F.C., Cabrera, N., and Burton, W.K., "Role of Dislocations in Crystal Growth," Nature, 163 (1949) 398.

62. Bacon, D.J. and Crocker, A.G., "The Elastic Energies of Dislocation Loops," Lattice Defects in Quenched Metals, Academic Press Inc., New York (1965).

63. Myers, A., "Some Elastic and Thermal Properties of Zirconium and Tungsten," Phil. Mag., 5 (1960) 927.

64. Bratine, W.J. and Winegard, W.C., "Internal Friction in Zirconium," Trans. AIME, 206 (1950) 186.

65. Fridel, J., Dislocations, Pergamon Press Ltd., London, (1964).

66. Douglas, D.L., "The Physical Metallurgy of Zirconium," Atomic Energy Rev., 1 (1963) 71.

67. Ohara, H., "Creep of Zirconium," Japan Inst. of Metals J., 22 (1958) 250.

68. Wolf, J.S., "Unpublished Results," University of Florida, Gainesville, Florida (1963).

69. Dorn, J.E. and Rajnak, S., "Nucleation of Kink Pairs and the Peierls Mechanism of Plastic Deformation," Trans. AIME, 230 (1964) 1052.

BIOGRAPHICAL SKETCH

Edward Philip Dahlberg was born August 8, 1937 in Chicago, Illinois. He attended Carl Schurz High School in Chicago. Under the auspices of the Ford Foundation he enrolled at Shimer College, Mount Carroll, Illinois, as an early entrant student, where he received his 12th grade certificate in June, 1954, and the degree of Bachelor of Arts in June, 1956. In June, 1959, he received the degree of Bachelor of Science in Science Engineering from Northwestern University, Evanston, Illinois. He received the degree of Master of Science in Materials Science from Northwestern University in September, 1960. From 1960 to 1963 he was employed as a research physical metallurgist at the Naval Research Laboratory in Washington, D. C. In September, 1963, he began studies for the doctorate at the University of Florida, Gainesville, Florida, with the aid of a College of Engineering Fellowship.

Edward Philip Dahlberg is married to the former Nancy Anne Moulton and is the father of three children, Amy, Susan and Frisk. He is a member of the American Society of Metals, American Institute of Mining and Metallurgical Engineers, Tau Beta Pi, and Sigma Xi.

This dissertation was prepared under the direction of the chairman of the candidate's supervisory committee and has been approved by all members of that committee. It was submitted to the Dean of the College of Engineering and to the Graduate Council, and was approved as partial fulfillment of the requirements for the degree of Doctor of Philosophy.

April, 1967

Dean, College of Engineering

Dean, Graduate School

Supervisory Committee:

R. E. Reed-Hill
Chairman

R. T. Duffy

John Haber

Lane J. Yoe

Craig Hartley